Published in final edited form as:

Cell. 2019 November 27; 179(6): 1393–1408.e16. doi:10.1016/j.cell.2019.10.025.

Periodic remodeling in a neural circuit governs timing of female sexual behavior

Sayaka Inoue[1], **Renzhi Yang**[3], **Adarsh Tantry**[1], **Chung-ha Davis**[4], **Taehong Yang**[1], **Joseph R. Knoedler**[1], **Yichao Wei**[1], **Eliza L. Adams**[4], **Shivani Thombare**[1], **Samantha R. Golf**[4], **Rachael L. Neve**[8], **Marc Tessier-Lavigne**[5], **Jun B. Ding**[6,7], **Nirao M. Shah**[1,2,9,*]

[1]Department of Psychiatry and Behavioral Sciences, Stanford University, Stanford, CA 94305, USA

[2]Department of Neurobiology, Stanford University, Stanford, CA 94305, USA

[3]Biology Program, Stanford University, Stanford, CA 94305, USA

[4]Neurosciences Program, Stanford University, Stanford, CA 94305, USA

[5]Department of Biology, Stanford University, Stanford, CA 94305, USA

[6]Department of Neurosurgery, Stanford University, Stanford, CA 94305, USA

[7]Department of Neurology, Stanford University, Stanford, CA 94305, USA

[8]Gene Delivery Technology Core, Massachusetts General Hospital Cambridge, MA 02139 USA

[9]Lead Contact

SUMMARY

Behaviors are inextricably linked to internal state. We have identified a neural mechanism that links female sexual behavior with the estrus, ovulatory phase of the estrous cycle. We find that progesterone receptor (PR) expressing neurons in the ventromedial hypothalamus (VMH) are active and required during this behavior. Activating these neurons however does not elicit sexual behavior in non-estrus females. We show that projections of PR+ VMH neurons to the anteroventral periventricular (AVPV) nucleus change across the 5 day mouse estrous cycle, with ~3-fold more termini and functional connections during estrus. This cyclic increase in connectivity is found in adult females but not males and regulated by estrogen signaling in PR+ VMH neurons. We further show that these connections are essential for sexual behavior in receptive females. Thus, estrogen-regulated structural plasticity of behaviorally salient connections in the adult female brain links sexual behavior to the estrus phase of the estrous cycle.

*Correspondence: nirao@stanford.edu.

AUTHOR CONTRIBUTIONS

Conceptualization, JBD, MTL, NMS, RY, SI; Funding, JBD, MTL, NMS; Investigation, AT, ChD, ELA, JBD, JRK, RLN, RY, SI, SRG, ST, TY, and YW; Supervision, JBD, MTL, NMS, and SI; Writing, JBD, NMS, RY, and SI.

DECLARATION OF INTERESTS

The authors declare no competing interests.

Graphic Abstract

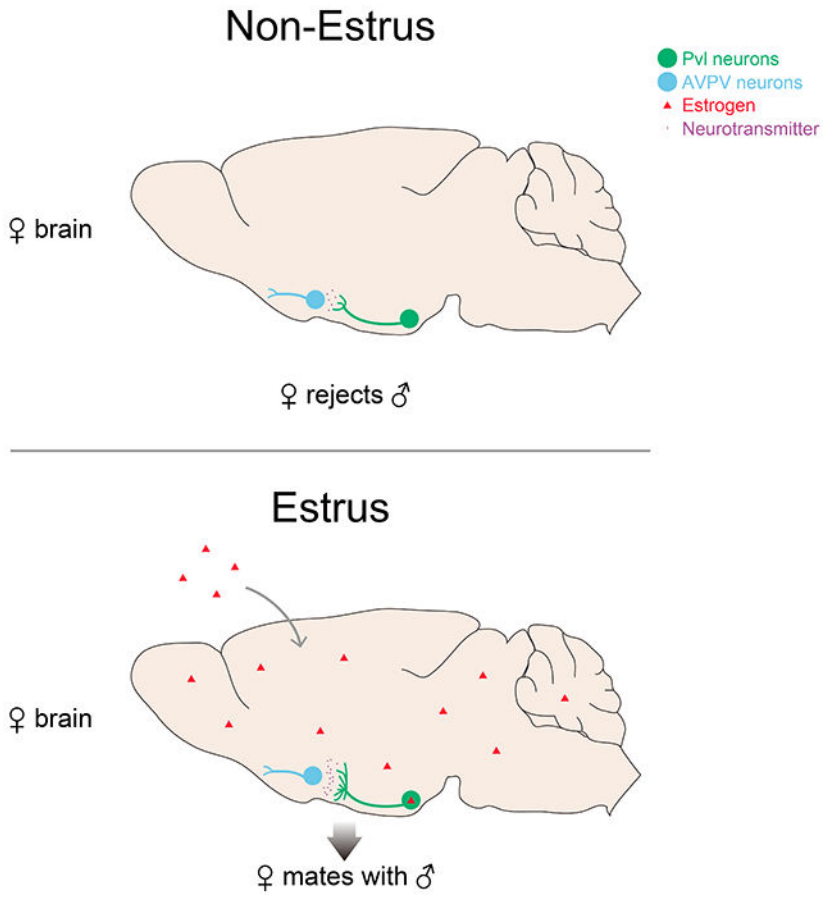

In Brief

Female mating behavior is coordinated with ovulation by estrogen-dependent anatomical and functional remodeling that increases the connections between key neurons in the hypothalamus of mice.

INTRODUCTION

Female sexual behavior is intimately linked with the estrous cycle in many species such that females are only receptive for a brief period at the estrus stage surrounding ovulation. This coincidence of female sexual receptivity with ovulation leads to extreme differences in behavioral ecology and reproductive strategies. For example, mice enter estrus and are receptive every 5 days whereas the giant panda is in estrus and receptive once a year, representing a naturally occurring ~70-fold variation in the potential to engage in sexual behavior (Allen, 1922; Lindburg et al., 2001). Such alliance between sexual behavior and ovulation can be adaptive because a reduction in non-productive mating is energetically efficient and lowers risk of predation, and productive mating during particular periods likely enhances survival of progeny.

The sex hormones 17β-estradiol (the most bioactive form of estrogens *in vivo*, and referred to as estrogen here) and progesterone released by the ovary are required for female sexual behavior and ovulation in many animals. The titers of these hormones in the circulation peak around estrus, at the time of female sexual receptivity and ovulation, whereas hormone levels subside to baseline, essentially undetectable levels at other stages of the estrous cycle in mice (DeLeon et al., 1990; Nelson et al., 1992). Estrogen and progesterone act reversibly in adult females to promote ovulation and sexual behavior, an action referred to as the activational effect of hormones (Arnold, 2009; Ring, 1944). For example, removal of ovaries in adult wildtype (WT) females abrogates receptivity and supplementing such females with estrogen and progesterone induces this behavior. These sex hormones signal through cognate nuclear hormone receptors estrogen receptor alpha (ERα or Esr1) and PR (or Pgr) that are also essential for ovulation and sexual behavior (Lubahn et al., 1993; Lydon et al., 1995; Rissman et al., 1997). The interplay between the pituitary-gonadal hormonal axis and physiological estrus (including ovulation) is well understood, including the developmental, organizational roles of sex hormones in enabling females to enter physiological and behavioral estrus (Brenner and West, 1975; Bronson, 1979; Kudwa et al., 2005; Adler et al., 1985). By contrast, neural pathways that link physiological estrus to female sexual behavior remain poorly characterized.

The ventrolateral part of the VMH (VMHvl) is important for female sexual behavior (Blaustein, 2008; Goy and Phoenix, 1963; Kendrick et al., 1995; Leedy and Hart, 1985; Mathews et al., 1983; Nomoto and Lima, 2015; Pfaff and Sakuma, 1979; Robarts and Baum, 2007; Swaab, 2003), and it contains a collection of PR+ neurons that is essential for female sexual behavior (Yang and Shah, 2014; Yang et al., 2013). These neurons co-express Esr1, and targeted ablation of PR+ VMHvl (Pvl) cells in adult females renders even estrus females unreceptive. Importantly, targeted ablation of Pvl neurons does not appear to alter the estrous cycle or other behaviors (Yang et al., 2013). Together, these findings demonstrate a central role for these cells in the display of female sexual behavior and show that functional manipulations of Pvl neurons decouple behavioral (female sexual receptivity) from physiological estrus. Such decoupling is to be expected if these cells modulate sexual displays but do not play a role in linking physiological estrus with female receptivity (Figure 1A). Alternatively, the targeted ablation of Pvl neurons, which profoundly and permanently reduced sexual receptivity, might have obscured a role of these cells in coupling female sexual behavior to physiological estrus.

In order to determine whether Pvl neurons play a role in linking receptive behavior to physiological estrus, we performed a series of acute functional manipulations in freely moving females. Surprisingly, although Pvl neurons are active and required during female sexual behavior, their activation did not elicit this behavior in unreceptive females. We find that estrogen signaling via Esr1 in the VMHvl elicits a ~3-fold increase in presynaptic termini of Pvl neurons in the AVPV. These presynaptic termini are functionally meaningful because optogenetically inhibiting them suppresses sexual behavior in receptive females. Thus, Pvl neurons are not only essential for the display of female sexual behavior, but they also play a critical role in linking this behavior to physiological estrus. More generally, our findings demonstrate large dynamic changes in connectivity in the adult female brain that

are regulated by estrogen and function to coordinate an innate behavioral program with physiological state.

RESULTS

Female Pvl neurons are active during various components of mating

To test whether Pvl neurons are active during female sexual behavior, we sought to express the calcium sensor GCaMP6s in female Pvl neurons and perform fiber photometry in $PR^{Cre/PL}$ mice (Cui et al., 2013; Gunaydin et al., 2014). We have previously generated PR^{Cre} and PR^{PL} mice harboring the transgenes *Cre recombinase* and *nuclear LacZ*, respectively, inserted 3' of IRES elements separately into the 3'UTR of *PR* in a gene conserving manner (Yang et al., 2013). These $PR^{Cre/PL}$ mice enable specific manipulation of PR+ cells in mice that are physiologically and behaviorally WT (Yang et al., 2013, 2017). As previously reported (Yang et al., 2013, 2017), delivery of virally encoded Cre-dependent mCherry resulted in mCherry expression in the vast majority of Pvl neurons in $PR^{Cre/PL}$ mice whereas no VMHvl cells were labeled in $PR^{PL/PL}$ controls (Figure 1B,C). In addition, most mCherry + neurons in the VMHvl co-expressed nuclear β-galactosidase (nβgal) (Figure 1D). The small percent of mCherry+ and nβgal− VMHvl neurons (9.3 ± 1.4%, n =3) reflects greater sensitivity in detecting a Cre-dependent transgene driven by strong promoters and from ≥1 viral genomes in comparison to expression of nβgal, which is inserted as a single-copy into the weakly transcribed *PR* locus (Yang et al., 2013, 2017). These results confirm previous work showing co-expression of Cre-dependent transgenes in genetically marked Pvl neurons *in vivo* (Yang et al., 2013, 2017) and allowed us to proceed with imaging calcium activity in Pvl neurons.

We targeted expression of a virally encoded GCaMP6s (AAV-flex-GCaMP6s) to Pvl neurons of PR^{Cre} females, removed ovaries (Ovx), and implanted an optic fiber over the VMHvl (Figure 1E–G). Ovx eliminates from circulation the estrus-inducing hormones estrogen and progesterone and enables comparison of females at polar ends of physiological estrus and receptivity by experimental supplementation with these hormones or vehicle (Table S1). Following recovery from surgery, we hormonally primed these females to be receptive and inserted them into the cage of a singly housed sexually experienced WT male (Ring, 1944; Wu et al., 2009). Entry into the cage led to a large increase in GCaMP6s fluorescence in these females (Figure 1H,I). Mice utilize chemosensory cues to interact with their environment, and we observed increases in GCaMP6s fluorescence when females chemoinvestigated (sniffed) the males (Figure 1J,K). GCaMP6s signal also increased when the WT male sniffed the female, indicating that her Pvl neurons were responding to tactile cues or shorter range volatile odors emanating from the male (Figure 1L,O). In mice, sexual behavior consists of multiple bouts of mounting and intromission (penetration) that can eventually culminate in ejaculation. Estrus females will often adopt an immobile receptive stance (lordosis) when the male mounts or intromits to enable mating to succeed (Harvey, 1651; Thompson and Edwards, 1971). GCaMP6s fluorescence increased in Pvl neurons during lordosis and essentially all mount and intromission events regardless of whether or not they resulted in lordosis (Figure 1M–O and Movie S1). In addition, we observed an increase in GCaMP6s fluorescence when the male ejaculated (peak $\Delta F/F = 0.065 \pm 0.01$,

Mean ± SEM, n=4) (Movie S1). Thus, Pvl neurons in receptive females are responsive to chemoinvestigation and various mating displays of both males and females. Surprisingly, Pvl neurons of Ovx, unprimed (and therefore unreceptive) females responded similarly when the female entered a male cage, during episodes of sniffing, as well as when the male attempted to mount her (Figure S1A–H and Movie S1). Sexually experienced males can occasionally intromit even with non-estrus females, and we observed corresponding increases in GCaMP6s fluorescence of unreceptive female Pvl neurons (Figure S1G,H). Non-estrus females do not lordose, and accordingly we could not determine if lordosis also increased GCaMP6s signal in Pvl neurons of unprimed females. In preliminary studies, we also observed that Pvl neurons of naturally cycling females showed comparable responses during mating regardless of whether the female was in diestrus or estrus (data not shown). Together, our findings show that, unexpectedly, Pvl neurons are active during exploratory and copulatory aspects of mating in receptive as well as unreceptive females.

To test if we would observe similar changes in Pvl activity when females were exposed to other cues, we inserted them into a cage containing a WT receptive female or an inanimate object (wooden block). Pvl neurons responded similarly to both stimuli regardless of whether or not females were primed to be in estrus (Figures 1H–K and S1I–P). Strikingly, these cells responded equivalently to the object and the WT female, and their response was significantly less than that observed toward males (Figure 1H–K). The differential and rapid response of Pvl neurons to entry into a male cage makes it unlikely to be simply a stress response; consistent with this notion, we did not observe any change in circulating corticotropin (ACTH) upon entry into the cage (Figure S1Q). In summary, our findings establish that female Pvl neurons respond preferentially during various interactions with a male, including mating routines, and that these responses are observed in both receptive and unreceptive mice.

Activity of Pvl neurons is necessary but not sufficient for female sexual behavior

We tested whether Pvl neurons acutely regulate female sexual behavior. We targeted a virally encoded Cre-dependent inhibitory DREADD (DREADDi) (Roth, 2016; Sternson and Roth, 2014) to Pvl cells of PR^{Cre} females and performed Ovx (Figures 2A and S2A). We induced estrus with hormonal priming and inserted these females into the cage of a WT singly housed male. The DREADD ligand CNO specifically elicited a marked diminution in sexual receptivity and an increase in rejection of male mating attempts (Figures 2B–D and S2B–E), with a corresponding ~4-fold reduction in the ability of WT males to ejaculate (Figure 2E). This chemogenetic reduction in female sexual receptivity demonstrates that ongoing activity of Pvl neurons is critical for mating behavior of receptive females.

We next tested if activation of Pvl neurons could elicit sexual receptivity in females. The excitatory DREADD (DREADDq) depolarizes membrane potential and increases spiking in Pvl neurons of both sexes (Yang et al., 2017). We therefore delivered virally encoded Cre-dependent DREADDq to the VMHvl of PR^{Cre} females, performed Ovx, and tested whether CNO elicited sexual receptivity (Figures 2F and S2F). Hormone induction of estrus leads to females who are highly sexually receptive, and we could not enhance this behavior further with CNO because of a ceiling effect (Figure S2G–J). We wondered whether we could

induce receptivity in primed females in a more sensitized setting. Accordingly, we tested whether activation of Pvl neurons in primed females was sufficient to elicit receptive behavior in the presence of males who did not mate. We therefore activated these cells in primed females and inserted them into the cage of a castrated male. However, the mere presence of a male who did not initiate any mating did not elicit sexually receptive behavior from primed females treated with saline or CNO (0/5 females showed lordosis). We also did not observe sexually receptive behavior upon chemogenetic activation of Pvl neurons in a separate cohort of primed females who were inserted into the cage of a castrate male whose dorsum was coated with urine from gonadally intact males (0/5 females showed lordosis). This latter set of castrate males bear the pheromonal profile of gonadally intact males but do not initiate mating. Thus, activation of Pvl neurons in primed females is not sufficient to elicit receptive behavior in the mere presence of males.

We next tested if activation of Pvl neurons could induce receptivity in Ovx, unprimed females. However, such females were unreceptive and rejected males, who were consequently unable to ejaculate (Figure 2G–J). CNO but not saline induced Fos in Pvl neurons of these females, showing that these cells were activated as expected (Figure S2K,L) (Yang et al., 2017). The dose of CNO (0.3 mg/kg) that we employed has also been shown to induce behavioral responses in DREADDq-expressing neurons of the VMHvl and other regions (Ray et al., 2011; Sasaki et al., 2011; Unger et al., 2015; Yang et al., 2017). Moreover, even a higher dose of CNO (15 mg/kg) did not elicit sexual receptivity (Figure S2M–P) in unprimed females. CNO typically elicits behavioral effects of CNO within 20-30 min, including in the VMHvl (Yang et al., 2017). Given the lack of sexual receptivity 30 min after CNO administration, we also tested a new cohort of Ovx, unprimed PR^{Cre} females expressing DREADDq in Pvl neurons 90 min after CNO administration. However, these females were equally unreceptive to mating attempts (Figure 2G–J).

We also tested whether optogenetic activation of Pvl neurons could induce sexual receptivity in Ovx, unprimed females. We targeted virally encoded Cre-dependent channelrhodopsin-2 (Fenno et al., 2011) (AAV-flex-ChR2:EYFP) to Pvl neurons of PR^{Cre} females, performed Ovx, and implanted optic fibers bilaterally over the VMHvl (Figures 2K and S2Q). Similar to chemogenetic activation, laser illumination (473 nm) did not elicit sexual receptivity in these females despite specifically inducing Fos in Pvl neurons (Figures 2L–O and S2R–W). The optogenetic parameters we employed (20 ms pulse, 20 Hz, 1 mW) elicit behavioral responses in females following stimulation of VMHvl neurons in other social settings (Lee et al., 2014). Thus, despite using validated parameters for activating Pvl neurons, we did not observe sexual receptivity in unprimed females. Moreover, increasing the laser power to 3 mW also did not induce sexual receptivity in a new cohort of Ovx, unprimed PR^{Cre} females expressing ChR2 in Pvl neurons (0/3 PR^{Cre} females showed lordosis and 0/3 WT stimulus males could ejaculate). It is possible that further optimization of chemogenetic or optogenetic activation of Pvl neurons might induce sexual receptivity in such females. Nevertheless, our current findings demonstrate that activity of Pvl neurons is required for female sexual behavior in receptive females, whereas experimental activation of these neurons does not induce this behavior in unreceptive females.

Female sex hormones drive structural plasticity of Pvl projections to AVPV

Our findings show that although Ovx, unprimed females are not sexually receptive, their Pvl neurons are active during exploration and male mating attempts, and further stimulation of these cells does not induce female sexual receptivity. Given the activational role of ovarian hormones in the estrous cycle, we wondered if projections of Pvl neurons varied across the estrous cycle. Pvl neuron projections are similar in most regions in the two sexes, but female Pvl neurons send more projections to the AVPV, a known hub of diverse female reproductive behaviors and physiology (Hellier et al., 2018; Scott et al., 2015; Simerly, 2002; Yang et al., 2013). To label projection termini of Pvl neurons in the AVPV, we targeted a Cre dependent, virally encoded mCherry fused to the synaptic vesicle protein synaptophysin (Syp:mCherry) to Pvl neurons and performed Ovx. We waited two weeks to allow Syp:mCherry to be transported to AVPV, then randomly delivered estrus-inducing hormones or vehicle and analyzed Pvl projections (Figure 3A,B). We observed a large increase in Syp:mCherry+ presynaptic termini in AVPV in primed females compared to unprimed females (Figure 3C). Although we employ high titer AAV vectors to deliver Syp:mCherry, there can be subtle variations in the number of transduced Pvl neurons. However, even following normalization for variability in viral transduction, we observed a ≥3-fold increase in mCherry+ presynaptic termini in AVPV in primed females (Figures 3D and S3A). We tested whether a different Cre-dependent reporter expressed under the control of a different constitutive promoter would also reveal hormone-dependent structural plasticity of Pvl neurons in AVPV. We co-expressed membrane GFP (mGFP) and mRuby fused to synaptophysin (Syp:mRuby) (Beier et al., 2015) in Pvl neurons and examined the AVPV (Figure S3B). We observed a similar ≥3-fold increase in mRuby+ presynaptic puncta in AVPV in primed compared to unprimed females (Figure S3C,D). Importantly, mGFP also labeled a larger area in AVPV in estrus females; the increase in mGFP labeled area was smaller than the increase in mRuby+ presynaptic termini, presumably because most of the axonal surface area is not part of the presynaptic zone (Figure S3C,G). We did not observe sex hormone driven changes in the other major projections of Pvl neurons to the preoptic hypothalamus (POA) and periaqueductal gray (PAG) (Yang et al., 2013) (Figures 3E,F and S3E,F,H,I). In summary, we observe a specific increase in the number of presynaptic termini of Pvl neurons in AVPV of primed females.

We next tested whether Pvl projections to AVPV were similarly plastic in adult males and regulated by activational action of sex hormones. The fewer projections of male Pvl neurons in AVPV could reflect a suppressive action of testosterone or the absence of estrus-inducing ovarian hormones. We targeted Syp:mCherry to the VMHvl of PR^{Cre} males, castrated (Cx) a subset, and examined Pvl projections in intact males (control), Cx males given vehicle, and Cx males primed to simulate estrus two weeks following delivery of the transgene (Figure 3G). We observed similar numbers of mCherry+ presynaptic termini in the male AVPV regardless of the hormonal regime (Figure 3H–K). This inability of estrus-inducing hormones to elicit an increase in presynaptic termini of male Pvl neurons in AVPV is consistent with previous work showing that these hormones also fail to elicit sexual receptivity-type behavior in adult males (Kudwa et al., 2005, 2006). Together, our findings demonstrate that estrus-inducing hormones elicit structural plasticity of Pvl projections to AVPV specifically in females.

Pvl projections to AVPV exhibit structural plasticity in naturally cycling females

Our results demonstrate that priming increases presynaptic termini of Pvl neurons in AVPV in females deprived of ovarian hormones for ~2 weeks. To test whether Pvl projections undergo structural changes in response to the endogenous changes in hormone titers across the 5-6 day cycle, we delivered Syp:mCherry to Pvl cells of PR^{Cre} females and did not perform Ovx. Two weeks after delivery of the transgene, we determined estrous stage by daily vaginal cytology (Figure 4A). Females are essentially completely sexually unreceptive during diestrus whereas they are receptive during the peri-ovulatory estrus stage. We therefore examined Pvl projections to the AVPV from females at these stages of the estrous cycle. We observed a ~2.7-fold increase in the number of mCherry+ presynaptic termini in AVPV when the females were in the sexually receptive estrus phase compared to the unreceptive, diestrus stage of the cycle (Figures 4B,C and S4A,B). As with females lacking ovaries (Figure 3), there was no difference in mCherry+ puncta in POA and PAG in estrus or diestrus females (Figure 4D,E). Together, our findings demonstrate a striking endogenous structural plasticity in Pvl projections to the AVPV, with more presynaptic termini when the intact female is in physiological and behavioral estrus.

Female sex hormones increase functional excitatory projections of Pvl neurons to AVPV

The vast majority (>99%) of Pvl neurons is glutamatergic, and correspondingly most mCherry+ presynaptic termini of Pvl neurons in the AVPV were labeled with vGlut2 (Figure S5A–C) (Hashikawa et al., 2017; Ng et al., 2009). We next tested if the increase in presynaptic termini of Pvl neurons in AVPV was functionally meaningful *in vivo* and in acute slice preparations. To test this *in vivo*, we targeted Cre-dependent DREADDq to Pvl neurons of PR^{Cre} females and performed Ovx. We then primed the females, activated Pvl neurons with CNO, and analyzed AVPV neurons for Fos induction (Figure 5A). There were more Fos+ AVPV neurons in females given CNO compared to saline in both primed and unprimed females (Figure 5B,C). Importantly, there were significantly more Fos+ AVPV neurons in primed than unprimed females given CNO even though there was no difference in Fos induction in Pvl neurons between these females (Figures 5B,C and S5D,E). Thus, the increase in presynaptic termini of Pvl neurons in AVPV corresponds to an increase in functional connectivity between these populations.

We next tested how female sex hormones impact synaptic transmission *ex vivo* using acute brain slices through the AVPV. We performed whole-cell patch clamp recording from AVPV neurons and examined mean frequency and amplitude of α-amino-3-hydroxy-5-methyl-4-isoxazolepropionic acid receptor (AMPAR)-mediated spontaneous miniature excitatory postsynaptic currents (mEPSCs) (Figure 5D,E). There was a significant increase of the frequency, but not amplitude, of mEPSCs in primed females (Figure 5F,G). To selectively examine the effects of the projection from PR+ VMHvl to AVPV neurons, we targeted virally encoded Cre dependent ChR2-mCherry to Pvl neurons of PR^{Cre} females, performed Ovx and recorded optogenetically evoked EPSCs (oEPSCs) in acute brain slices through the AVPV (Figures 5H and S5F,G). We found that the peak amplitude of oEPSCs in AVPV neurons was larger by >2.5-fold in primed compared to vehicle treated females (Figure 5I,J). Together, these data suggest that ovarian sex hormones enhance excitatory projections from

Pvl to AVPV by increasing the number of glutamatergic synapses formed onto AVPV neurons without affecting the strength of individual synapses.

Pvl projections to AVPV are essential for ongoing female sexual behavior

We tested the importance of the estrus-coupled increase in Pvl presynaptic termini in AVPV to female sexual behavior using optogenetics. We targeted virally encoded eNpHR3.0 or EYFP to Pvl neurons in PR^{Cre} females, performed Ovx, and implanted an optic fiber dorsal to the AVPV (Figure 6A,B). We switched on the laser (5mW, 593.5nm) or kept it switched off and inserted the primed female into the cage of a WT sexually experienced male. Continuous illumination of Pvl projections in the AVPV reduced sexual behavior in females expressing eNpHR3.0 in Pvl neurons (Figures 6C–F and S6A). There was a >6-fold reduction in lordosis, and the females also spent more time rejecting males. There was a corresponding decrease in the percent of male mounts that successfully transitioned to intromission and a >5-fold reduction in the percent males who could ejaculate with experimental females. The reduction in sexual behavior in females expressing eNpHR3.0 did not reflect toxicity resulting from overexpression of this hyperpolarizing pump because, in the absence of laser illumination, these experimental females were as sexually receptive as control females (Figure S6B–E).

We next tested whether intermittent inhibition of Pvl projections would reduce ongoing displays of sexual receptivity. We prepared a new cohort of PR^{Cre} females for optogenetic inhibition as described above (Figure 6A,B). We switched the laser on and immediately inserted the primed female into the cage of a WT sexually experienced male. In these tests, we cycled laser illumination every 5 min (5mW, 593.5nm) and analyzed behavioral performance in the presence or absence of light. We observed a striking and specific reduction in sexual receptivity during laser illumination compared to when the laser was switched off in females expressing eNpHR3.0 in Pvl neurons (Figures 6G–J and S6F–J, and Movie S2). With the laser on, females rejected males more, lordosed less, and correspondingly, males were unable to ejaculate. These deficits were comparable to those observed with continuous inhibition (Figure 6C–F), and they demonstrate that ongoing activity in Pvl projection termini in AVPV plays a critical role during female sexual behavior.

Estrogen signaling controls estrus-linked increase in Pvl presynaptic termini in AVPV

Behavioral estrus is typically induced by providing estrogen and progesterone sequentially to mimic endogenous hormone titers. However, PR expression in Pvl neurons is only induced in the presence of estrogen signaling via Esr1 (Musatov et al., 2006), indicating that estrogen signals upstream of progesterone to elicit female sexual behavior. In addition, progesterone appears to play a subtle role in activating female sexual behavior, because estrogen alone is sufficient to induce this behavioral display at near-maximal intensity (Rissman et al., 1997). We therefore tested if priming with estrogen alone would suffice to increase presynaptic termini of Pvl neurons in the AVPV. We targeted Syp:mCherry to Pvl neurons, performed Ovx, and imaged mCherry+ presynaptic termini within the AVPV (Figure 7A). In comparison to vehicle treated females, priming with estrogen alone induced a ~3-fold increase in the number of mCherry+ presynaptic termini in AVPV but not POA or

PAG (Figures 7B,C and S7A,B). These estrogen-elicited changes are comparable to those observed in females that are primed with estrogen and progesterone or cycling naturally (Figures 3C,D, 4B,C, and 7B,C) (p=0.66, Kruskal-Wallis test). Thus, estrogen is sufficient to increase presynaptic termini of Pvl neurons in AVPV.

These results raise the question of whether estrogen signaling is required in adult Pvl neurons for structural plasticity of their projection termini in the AVPV. Esr1 is expressed in the VMHvl, where it is required for female sexual behavior, and Pvl neurons express Esr1 (Musatov et al., 2006; Xu et al., 2012; Yang et al., 2013). We therefore decided to delete Esr1 in adult Pvl neurons and to examine their projections in AVPV in estrus females. We first tested whether other neurons in the vicinity of Pvl cells also elaborate projections to the AVPV. Targeting a virally delivered Syp:mCherry whose expression was switched off (Cre-off Syp:mCherry) in Cre+ neurons labeled a large number of mCherry+ cells in the VMH and adjacent regions (Figures 7D and S7C) of PR^{Cre} females. However, we observed few, if any, mCherry+ puncta within the AVPV (Figures 7E,F and S7D,E), indicating that neurons adjacent to Pvl cells do not project to the AVPV. We tested this conclusion using an orthogonal approach. We ablated adult Pvl neurons in PR^{Cre} females using a Cre-dependent, designer caspase that induces cell autonomous apoptosis (Figure S7F) (Yang et al., 2013). We then delivered a fluorescently-labeled cholera toxin B (CTB), a retrograde tracer, to the AVPV in these females. We observed many CTB+ neurons in the VMHvl of WT females who had also been injected with the Cre-dependent designer caspase, but CTB+ neurons were essentially absent in the VMH of PR^{Cre} females in whom we had ablated Pvl neurons (Figure S7G,H). Together these findings demonstrate that the vast majority, if not all, AVPV projections from the VMH emanate from Pvl neurons.

We then targeted Cre or control vector unilaterally and a constitutively expressed Syp:mCherry bilaterally to the VMHvl of females homozygous for a loxP-flanked *Esr1* allele ($Esr1^{Flox/Flox}$) (Feng et al., 2007), performed Ovx, and examined mCherry+ presynaptic termini in the AVPV following hormonal priming (Figures 7G and S7I,J). There were significantly fewer mCherry+ presynaptic termini in the AVPV ipsilateral to the side with a Cre-mediated deletion of *Esr1* in the VMHvl (Figures 7H,I and S7I–L). The fold reduction in the density of Pvl presynaptic termini in AVPV upon deletion of Esr1 in VMHvl was comparable to that observed in females with naturally or experimentally low estrogen in the circulation (Fold reduction in density of mCherry+ Pvl presynaptic termini in AVPV: Esr1 deleted in VMHvl, 0.38 ± 0.09; Vehicle treated Ovx female, 0.27 ± 0.06; Diestrus female, 0.34 ± 0.1; p = 0.6, Kruskal-Wallis test; data from Figures 3C,D, 4B,C, and 7H,I). Together, these findings indicate that estrogen signals predominantly via Esr1 in VMHvl neurons to control the estrus-induced increase in presynaptic termini of Pvl neurons in the AVPV. In summary, our results demonstrate that estrogen is necessary and sufficient to drive increase of presynaptic termini of Pvl neurons to the AVPV.

DISCUSSION

In many animals, females are sexually active only during the period when they are fertile. Pvl neurons are essential for female sexual receptivity but not for ovulation, suggesting that they do not regulate the link between behavioral and physiological estrus. However, we find

that in fact Pvl neuron activity is not sufficient to trigger sexual receptivity in non-estrus states because structural plasticity of presynaptic termini of these cells restricts behaviorally meaningful functional connectivity with AVPV neurons to estrus females. Thus, Pvl neurons, which are critical for female sexual receptivity, are also important for synchronizing this behavior with estrus. Both female sexual behavior and ovulation occur at a time when estrogen peaks in the circulation. We show that estrogen signaling via Esr1 is required for the structural plasticity that enables Pvl neurons to communicate effectively with their postsynaptic partners in AVPV. Previous work indicates that estrogen signaling in these cells is required for female sexual behavior (Barfield and Chen, 1977; Blaustein et al., 1994; Davis et al., 1982; Musatov et al., 2006; Pleim et al., 1989; Rubin and Barfield, 1980). In other words, estrogen not only promotes ovulation, but it also acts in Pvl neurons to trigger structural plasticity of their projections to AVPV and to elicit sexual receptivity. In summary, our studies show that physiological estrus is linked to female sexual behavior by large scale presynaptic structural plasticity of the neural pathway that is also required for the behavior.

Sexual behavior and fertility

Among vertebrate species, there are at least three types of female mating strategies (Brenner and West, 1975; Adler et al., 1985): mating is restricted to a peri-ovulatory period (mice), mating induces ovulation (rabbits), and mating is decoupled from fertility (humans). The VMH is thought to regulate female sexual receptivity across a wide range of vertebrates, including humans, indicative of a deeply conserved pathway underlying this behavior (Blaustein, 2008; Goy and Phoenix, 1963; Kendrick et al., 1995; Leedy and Hart, 1985; Mathews et al., 1983; Pfaff and Sakuma, 1979; Robarts and Baum, 2007; Swaab, 2003). It is possible that structural plasticity of VMH projections to the AVPV is an adaptive specialization that is observed only in species in whom mating is restricted to the peri-ovulatory period. Alternatively, such plasticity may also be observed in animals in whom mating induces, or is decoupled from, ovulation. In fact, MRI studies suggest periodic changes in the human hypothalamus and other brain regions across the menstrual cycle (Baroncini et al., 2010; Pletzer et al., 2010). In these instances, such plasticity may serve other functions or it may be bypassed by other circuit mechanisms (Ishii et al., 2017; Osakada et al., 2018). It will be interesting to determine whether plasticity of presynaptic termini of Pvl neurons in AVPV also restricts female sexual behavior to the peri-ovulatory period in other species in whom this behavior and physiology are coordinated similar to mice. It is possible that distant vertebrate groups have evolved distinct mechanisms to link sexual receptivity to the window of fertility.

Hormones and plasticity

Sex hormones and their metabolites have been implicated in shaping circuit architecture and neurosecretory processes during development or adult life in many species (Balthazart and Ball, 2016; Chan et al., 2011; Clasadonte and Prevot, 2018; Cooke and Woolley, 2005; Fernald, 1995; Frankfurt et al., 1990; Konishi, 1989; Konishi and Akutagawa, 1985; Maruska and Fernald, 2013; Montagnese et al., 1990; Morris et al., 2004; Reisert et al., 1987; Toran-Allerand, 1976). In the adult mammalian brain, for example, there are estrous cycle driven morphological and functional changes in dendritic spines in hippocampus and

cortex (Luine and Frankfurt, 2013; Maguire and Mody, 2009; Tuscher et al., 2016; Wang et al., 2018; Woolley et al., 1990). Given the broad roles of these neurons in learning and memory and other behaviors, it has been difficult to link these morphological changes with discrete behavioral outcomes. In addition, whether these changes require Esr1 or other estrogen receptors in an autonomous or non-autonomous manner is unknown. More recently, estrogen and progesterone have been shown to act on chemosensory neurons and reward pathways to influence the attraction of female mice to males (Dey et al., 2015; McHenry et al., 2017). Our results show that any increase in attraction of estrus females toward a male suitor can only be consummated in the presence of functional connections between Pvl and AVPV neurons. These findings suggest a model wherein estrus hormones drive females to interact with males and subsequently to display sexual receptivity during mating. Such coordinated hormone action probably functions to increase the likelihood in the wild that an estrus female will approach a male and successfully mate with him.

The estrus-induced increase in connections between Pvl and AVPV neurons suggests a mechanism whereby activity of Pvl neurons is translated into behavioral action. Pvl neurons are active during mating attempts by the male irrespective of whether or not the female is in estrus. Nevertheless, the female is only sexually receptive when she is in estrus. Hormonal surges of estrogen and progesterone related to estrus could change gene expression in Pvl neurons to facilitate lordosis. However, receptivity cannot be induced by experimental activation of Pvl neurons in non-estrus females. Together, these findings suggest that the absence of estrus-induced connectivity between Pvl and AVPV neurons constitutes a physical circuit block to receptive behavior. Such state-dependent physical circuit blocks afford a mechanism that regulates transfer of information across a neural circuit that can appear physically contiguous by standard circuit mapping approaches. We observed reduced, but not absent, spontaneous and evoked activity of AVPV neurons postsynaptic to Pvl neurons in non-estrus females, suggesting some degree of connectivity between these neurons. The addition of new synapses on to these AVPV neurons may allow effective transmission of Pvl activity to downstream motor pathways that control receptive behavior. Alternatively, the circuit block may be relieved in estrus by formation of connections on to a different class of AVPV neurons. Regardless of the nature of the block, our findings do not exclude additional circuit checkpoints for lordosis or the existence of parallel or downstream circuit elements that can bypass the barrier imposed by this neural pathway.

Plasticity of neural circuits in the adult brain

With some exceptions, most studies on synaptic plasticity have performed electrophysiological and morphological characterization of spines and dendrites in learned behaviors (Bailey and Kandel, 2008; Hart and Hobert, 2018; Hu et al., 2007; Kauer and Malenka, 2007; Liu et al., 2017; Mysore et al., 2008; Nicoll, 2017). By contrast, we have identified ongoing large scale axonal reorganization in a subcortical mammalian circuit that mediates innate behavior. We find significant structural presynaptic plasticity in the pathway between Pvl and AVPV neurons that occurs every few days in the adult female brain in response to ovarian hormones. It will be interesting to determine whether these different forms of synaptic plasticity employ similar molecular mechanisms. Pvl neurons collateralize such that individual neurons that project to AVPV also project to other target regions (Lo et

al., 2019). We observed estrous state-dependent changes in projections to AVPV but not POA or PAG, indicating that the structural plasticity of Pvl termini is restricted to specific projection targets. Such projection target specific plasticity renders it difficult to examine the specific role of Esr1 in regulating presynaptic plasticity of projections to AVPV and female sexual behavior. The AVPV contains a diversity of neuronal subtypes and the identity of the AVPV neurons postsynaptic to Pvl neurons is unclear. Whether these postsynaptic AVPV neurons undergo corresponding cyclic changes on their dendritic surface is an open question. Neither castration nor administration of estrus-inducing hormones could elicit structural plasticity in adult male Pvl neurons. The vast majority of Pvl neurons expresses Esr1 in both sexes, indicating that estrus hormone induced plasticity of projections to the AVPV in females but not males does not simply reflect absence of Esr1 in male Pvl neurons (Yang et al., 2013). It is likely that the ability of this pathway to rewire significantly in adults is developmentally hardwired into the female but not male brain. Such sex differences in developmental hardwiring could be reflected in sex differences in gene expression downstream of Esr1 that enable plasticity of projections to the AVPV in females but not males. In closing, we have uncovered large scale periodic structural plasticity in a genetically defined neural circuit that coordinates the estrous cycle with female sexual behavior. Our findings raise the possibility that neural circuits that regulate other innate behaviors, and are therefore also developmentally hardwired into the brain, can be re-wired in the adult mammalian brain.

STAR*METHODS

LEAD CONTACT AND MATERIALS AVAILABILITY

Further information and requests for resources should be directed to and will be fulfilled by the Lead Contact, Nirao Shah (nirao@stanford.edu). This study did not generate new unique reagents.

EXPERIMENTAL MODEL AND SUBJECT DETAILS

Mice—Animal studies were performed following Institutional Animal Care and Use Committee guidelines and protocols. Adult mice 10-24 weeks of age were used in all studies. Mice were housed under a reversed 12:12 hr light:dark cycle and water and food were available ad libitum. Mice bearing PR^{Cre}, PR^{PL}, $Esr1^{fox}$, and $Gadl^{EGFP}$ alleles have been described previously and were bred in our colony (Feng et al., 2007; Tamamaki et al., 2003; Yang et al., 2013). WT females were purchased from Jax (C57B16/J), and WT males (B6129SF1/J) used as stimulus animals in tests of sexual receptivity were bred in the animal facility or purchased from Jax. We found that female but not male projections of Pvl neurons to AVPV exhibited remodeling in response to ovarian hormones.

Viruses—AAV-EF1a-flex-hM3DDq:mCherry (serotypes 1 or DJ), AAV-EF1a-flex-hM4DDi:mCherry (serotypes 1 or DJ), and AAV-EF1a-flex-mCherry (serotype 1), AAV-EF1a-flex-taCasp3-TEVp (serotype DJ), AAV-EF1a-DIO-hChR2(H134R):mCherry (serotype 2), AAV-EF1a-DIO-eNpHR3.0:EYFP (serotype 2), AAV-EF1a-DIO-EYFP (serotype 2) were purchased from the UNC Vector Core or custom packaged by the UNC Vector Core. AAV-EF1a-DIO-hChR2(H134R):EYFP and AAV-Syn-flex-GCaMP6s (both of

serotype 1) were purchased from the Penn Vector Core or Addgene. AAV-EF1a-DO-Syp:mCherry and AAV-EF1a-Syp:mCherry (both of serotype 8.2) were purchased from the MGH viral core. AAV-EF1a-DIO-Syp:mCherry (serotype 1) and AAV-Syn-flex-mGFP-2A-Syp:mRuby (serotype DJ) were custom packaged by Virovek (Hayward, CA). Lenti-hSyn-Cre-EGFP and Lenti-hSyn-DCre-EGFP (VSVG pseudotype) were purchased from the Stanford Viral core (Cao et al., 2011). AAV titers were 1.5 x 10^{12} – 2.5 x 10^{13} genomic copies/mL, and lentivirus titers were 2.5 x 10^{7} – 5 x 10^{8} genomic copies/mL.

METHOD DETAILS

Stereotaxic Surgery—Viruses were stereotaxically delivered to the brains of mice at 2-4 months of age as described previously (Yang et al., 2013, 2017). In brief, virus was delivered bilaterally (0.8μL of AAV-flex-hM4DDi:mCherry, AAV-flex-hM3DDq:mCherry, AAV-flex-mCherry, AAV-DIO-ChR2-EYFP, AAV-DIO-ChR2:mCherry, AAV-DIO-eNpHR3.0:EYFP, AAV-DIO-EYFP, AAV-flex-taCasp3-TEVp, or 0.2μL of AAV-DIO-Syp:mCherry, AAV-flex-mGFP-Syp:mRuby, AAV-DO-Syp:mCherry, AAV-Syp:mCherry) or unilaterally (0.6 μL of AAV-flex-GCaMP6s, Lenti-hSyn-Cre:EGFP, Lenti-hSyn-EGFP) at 100 nL/min with a Hamilton syringe using a micropump. Immediately after surgery, mice were placed on a heated pad individually and then returned to their home cage following recovery from anesthesia. Animals were allowed at least 2 weeks of recovery following surgery prior to being tested in behavioral assays.

For optogenetic experiments and fiber photometry imaging, mice were also implanted with a fiber optic cable at the time of virus injection as described previously (Bayless et al., 2019). In brief, cannulas for optogenetics were made from 200 μm core fiber optic (NA 0.39) and 1.25 μm ceramic ferrule. For ChR2-mediated activation of Pvl neurons, cannulas were implanted bilaterally over the VMHvl. For eNpHR3.0-mediated suppression of axon termini of Pvl neurons, a midline cannula was implanted dorsal to the AVPV as previously described (Scott et al., 2015). In brief, cannulas for fiber photometry were made from 400 μm core fiber optic (NA 0.48) and ceramic ferrule and implanted unilaterally over the VMHvl. Adhesive dental cement (Parkell Inc) was used to secure ferrules to the skull. We performed Ovx on mice during viral delivery at the time of stereotaxic surgery unless otherwise noted. Following Ovx, mice were hormonally primed with estrogen on days 1 (10 μg in 100 μL sesame oil) and 2 (5 μg in 50 μL sesame oil) following this surgery. This enables estrogen signaling to induce PR expression in Pvl neurons, thereby permitting expression of the virally encoded Cre-dependent transgene.

We used the following stereotaxic coordinates (in mm): VMHvl (−1.3 A/P, ±0.78 M/L, −5.75 D/V for virus; −5.45 D/V for fiber optic cable), AVPV (+0.5 A/P, ±0.18 M/L, −5.4 D/V for virus; −5.15 D/V for fiber optic cable).

Hormone Priming—Unless otherwise mentioned we used Ovx females. Estrus was induced as described previously (Wu et al., 2009; Yang et al., 2013). Briefly, we delivered subcutaneously 10 μg of 17 β-estradiol benzoate (Sigma) in 100 μL of sesame oil on day −2, 5 μg of 17 β-estradiol benzoate in 50 μL of sesame oil on day −1, and 50 μg of progesterone (Sigma) in 50 μL of sesame oil on day 0, the day of testing. For estrogen alone priming

(Figure 7), females received estrogen as above. Control females received identical volumes of vehicle (sesame oil) for all studies. Females were behaviorally tested or perfused for histological analysis 4-6 hours after the last injection of hormone or vehicle.

Hormone titers—Serum ACTH level was measured using an ELISA kit (DRG) following the manufacturer's instructions. Mice were anesthetized 20 s after entry into the test cages and cardiac blood was collected. For the home cage control condition, the female was picked up and put back down in her home cage, anesthetized 20 s later, and blood was collected as described above. The 20 s time point was chosen for blood collection because the peak fluorescent change driven by social interaction was achieved at ~20 s after entry into a test cage (Figure 1H).

For estrogen and progesterone titers, cardiac blood from females was collected at the time of perfusion, and serum estrogen and progesterone levels were measured using an ELISA kit (Cayman) following the manufacturer's instructions.

Behavioral Assays—Behavioral assays were performed in the dark cycle (≥1 hr after lights out), recorded at 30 frames per second using camcorders under infrared illumination. Animals were group housed by sex after weaning. Females can exhibit low levels of sexual receptivity during the first mating experience (Thompson and Edwards, 1971; Xu et al., 2012), and to reduce variability in behavior, we subjected all females to be tested behaviorally (chemogenetics, optogenetics, fiber photometry) to a round of mating experience with a WT sexually experienced male. In this setting, we primed the female, inserted her into the male's cage for 30 min, and verified that mounting and intromission occurred. Following this, females were tested and analyzed for behavioral performance in mating tests as described in the text (Figures 1, 2, and 6). Mating tests were spaced ≥7 days apart to allow hormone levels to subside prior to estrus induction for the next assay.

Videos were manually annotated using the software ScoreVideo (Wu et al., 2009; Xu et al., 2012; Yang et al., 2013, 2017). Receptivity index was calculated by dividing the number of intromissions by the number of mounts displayed by the male. In contrast to the lordosis quotient, this metric provides a measure of success in transitioning from mounting to intromission. Rejection behavior was defined by the display of rejecting posture (running or walking away and rearing up against male) during a mount attempt. Lordosis was defined by the display of a concave-arched back posture while braced on all four legs during a mount or intromission. Lordosis quotient was calculated as follows: (# lordosis)/(# male mount or intromission).

Chemogenetics—Chemogenetic studies were performed as described previously (Unger et al., 2015; Yang et al., 2017). In brief, for hM4DDi (DREADDi) experiments, the Ovx female was primed. For hM3DDq (DREADDq) experiments, Ovx females were not primed. CNO stock solution was prepared by dissolving CNO (Enzo) in sterile saline at 5 mg/mL, kept as frozen aliquots, and freshly diluted with sterile saline prior to intraperitoneal (IP) administration. The final dose of CNO for mCherry, hM4DDi and hM3DDq studies was 15 mg/kg, 15 mg/kg and 0.3 mg/kg respectively, unless mentioned otherwise. The order of saline (vehicle) or CNO administration was counterbalanced across animals. Assays were

initiated 30 or 90 min after IP injection of saline or CNO. To examine DREADDq-mediated induction of Fos in the AVPV and VMHvl, animals were perfused 90 min after intraperitoneal (IP) administration of saline or 0.3 mg/kg of CNO.

***In vivo* optogenetics—**To activate Pvl neurons, AAV-EF1a-DIO-ChR2:EYFP was delivered bilaterally into the VMHvl. Control females received AAV-EF1a-DIO-EYFP injection. At the time of viral injection, 200 μm core, 0.39 NA optic fibers (Thorlabs) were bilaterally implanted 0.3 mm dorsal to the VMHvl, and Ovx was performed. Mice were allowed to recover 4 weeks before experiments. Then they were hormonally primed, habituated to the optogenetics setup, and received a mating experience for 30 min as described above. On the test day, immediately after the female was inserted into WT male's cage, we switched on the laser (473 nm, Optoengine). The 1 mW light power exiting the fiber tip is predicted to have an irradiance of 1.5~2.6 mW/mm^2 at the VMHvl (predicted irradiance values: https://web.stanford.edu/group/dlab/cgi-bin/graph/chart.php). We have also tested females under a regime of 3mW laser illumination, but did not observe any increase in sexual receptivity. To examine Fos induction in the VMHvl by ChR2 activation, animals received 5 min laser illumination (20ms pulses at 20Hz, 1mW) and were perfused 60 min later.

To inhibit axonal termini of Pvl neurons in AVPV, AAV-EF1a-DIO-eNpHR3.0:EYFP was delivered bilaterally into the VMHvl. Control females received AAV-EFla-DIO-EYFP into the VMHvl. At the time of viral injection, a 200 μm core, 0.39 NA optic fiber (Thorlabs) was implanted 0.1~0.25 mm dorsal to the AVPV {coordinates from (Scott et al., 2015)}, and Ovx was performed. Mice were tested ≥8 weeks after injection to allow efficient expression of eNpHR3.0 in axonal termini. They were habituated to the optogenetics setup and also received a mating experience with a WT male for 30 min as described above. On the test day, the laser (593.5nm, Optoangine) was switched on immediately after inserting the primed female into the male's cage. For continuous inhibition of Pvl neurons, laser illumination stayed on throughout the assay. As the internal control, the same mouse received another test without any laser illumination. For intermittent inhibition of Pvl neurons, laser illumination was delivered for 5 min every 5 min throughout the assay. The light power exiting the fiber tip was 5 mW, which is predicted to have an irradiance of 5~11mW/mm^2 at the AVPV. Illumination emanating from the fiber optic likely also inhibits Pvl fibers lateral to the AVPV, and these may also contribute to the reduction in female sexual behavior. The specific role of the Pvl-AVPV pathway can be revealed in future studies following development of anterograde trans-synaptic tracing tools to enable functional manipulations of AVPV cells postsynaptic to Pvl neurons. Nevertheless, given the role of AVPV neurons in female reproductive behavior and physiology, our findings strongly support the notion that Pvl projections to the AVPV regulate this behavior.

Fiber photometry—Fiber photometry was conducted essentially as described previously (Bayless et al., 2019; Chen et al., 2015). In brief, AAV-flex-GCaMP6s was injected unilaterally into the VMHvl. At the time of virus injection, a 400 μm core, 0.48NA optical fiber was implanted dorsal to the VMHvl, and Ovx was performed. Mice were allowed to recover at least 3 weeks before experiments. Then they were hormonally primed, habituated

to the photometry setup, and received a mating experience with a WT male for 30 min as described above. On the test day, to acquire baseline fluorescence, the female was first recorded in her homecage for 10 min. Then she was inserted into a cage containing a stimulus (WT male, WT estrus female, or wooden block) for 30 min. The order of behavior testing was first with WT male, second with WT female, and then with the object. Vehicle or primed conditions were counterbalanced.

Fiber photometry recordings were made using previously described equipment (Bayless et al., 2019; Chen et al., 2015). Briefly, a 473 nm laser diode (Omicron Luxx) was placed upstream of an optic chopper that was run at 400 Hz and then passed through a GFP excitation filter (Thorlabs). This signal was then reflected by a dichroic mirror (Semrock) and coupled through a fiber collimation package (Thorlabs) into a home-made patchcord. Fluorescence output was filtered through a GFP emission filter (Thorlabs) and focused by a convex lens (Thorlabs) onto a photoreceiver (Newport). The signal was outputted into a lock-in amplifier and then digitized with LabJack U6-Pro and recorded using software provided by LabJack at 250 Hz sampling rate.

All data analysis was performed in MATLAB. Behavioral video files and fiber photometry data were time-locked via a light flash present in both datasets that was initiated by a pulse generator (Doric). To reduce random noise, signals were first filtered by moving average filter. Then signals were normalized to the median fluorescent of the 10 min baseline period in the experimental animal's homecage. For peri-event time plots (PETP), the median value of fluorescent F_0 was calculated from a 5 sec window prior to each behavioral event except initial response and was used as the normalization factor to calculate change in fluorescence from baseline. This 5 sec window was set to avoid overlap of each behaviors in total 10 sec PETP window we analyzed. We excluded data from analysis if there was an overlap of behaviors within this time window. Then $\Delta F/F$ was calculated by subtracting F_0 from each fluorescent value. The peak fluorescence change (peak $\Delta F/F$) was calculated within the 5 sec window after onset of behavior. We confirmed that the latency to achieve peak AF/F is shorter than 5 sec for all behaviors except the initial response upon entry into a test cage (data not shown). For PETP of this initial response, a 40 sec window was used to calculate peak $\Delta F/F$ because peak fluorescence was achieved in ≤40 sec after entry.

General histological procedures—For histological analysis, animals were perfused with 4% paraformaldehyde, and the brains were dissected and post-fixed overnight in 4% paraformaldehyde. Brains were sectioned at 65 μm thickness using a vibrating microtome (Leica) and immunostaining was performed as described previously (Yang et al., 2013, 2017). In brief, sections were collected in PBS, blocked 1 hr in PBS containing 10% donkey serum and 0.1% Triton X100, incubated overnight at 4°C using primary antibodies described below in PBS containing 1% donkey serum and 0.1% Triton X100, washed 3 times in the same solution without antibodies (30 min per wash), labeled at room temperature for 2 hrs with secondary antibodies described below, washed 3 times in the same solution without antibodies (30 min per wash), washed twice in PBS containing 0.1% Triton X100 (30 min per wash), and rinsed three times with PBS.

Primary antisera used are rat anti-RFP (Chromotek; 1:2,000), rabbit anti-Fos (Santa Cruz Biotechnology; 1:500), chicken anti-b-galactosidase (Abcam; 1:3,000), sheep anti-GFP (Bio Rad; 1:2000), rat anti-mCherry (Life Sciences; 1:2000), rabbit anti-Esrl (Millipore, 1:10,000), and guinea pig anti-vGlut2 (Synaptic Systems; 1:1000). Secondary antisera used are: Cy3 donkey anti-rat (Jackson ImmunoResearch; 1:800), Alexa Fluor 488 donkey anti-rabbit (Jackson ImmunoResearch; 1:300), Cy3 donkey anti-chicken (Jackson ImmunoResearch; 1:800), Alexa Fluor 488 donkey anti-chicken (Jackson ImmunoResearch; 1:300), Alexa Fluor 488 donkey antisheep (Jackson ImmunoResearch; 1:300), and Alexa Fluor 647 donkey anti-guinea pig (Jackson ImmunoResearch; 1:500). Sections were counterstained with DAPI (0.2 mg/mL) prior to mounting on to slides.

Sections were imaged via confocal microscopy (Zeiss LSM780 or LSM880). Use of AAV vectors routinely enables infection of ≥90% of Pvl neurons in all animals that survive surgery and behavioral testing (Yang et al., 2013, 2017). Neurons were quantified using Photoshop or NIH ImageJ software as follows. We quantified the fraction of Pvl neurons expressing various transgenes (ChR2, DREADDi, DREADDq, eNpHR3.0, Syp:mCherry, Syp:mRuby, mGFP, mCherry, EGFP, EYFP) as follows. We enumerated transgene+ neurons in PR^{Cre} females in the middle three (out of a total of nine) histological sections through the VMHvl because they contain the majority of Pvl neurons (57.8 ± 4.1%, n = 3). This number was then divided by the number of nβgal+ Pvl neurons in the middle three sections through the VMHvl of $PR^{PL/PL}$ mice to obtain an estimate of the fraction of Pvl neurons expressing the virally encoded transgene. In agreement with previous reports, this viral strategy yielded infection of 99 ± 2% of Pvl neurons (Figure 1, 102 ± 10% of Pvl neurons expressed GCaMP6s; Figure 2, 104 ± 11% of Pvl neurons expressed DREADDi, 97 ± 5% of Pvl neurons expressed DREADDq, 94 ± 10% of Pvl neurons expressed ChR2, 92 ± 19% of Pvl neurons expressed EYFP; Figure 3, 89 ± 14% and 90 ± 7% of Pvl neurons expressed Syp:mCherry in vehicle treated and primed Ovx females; Figure 3, 114 ± 15%, 90 ± 13%, and 98 ± 16% of Pvl neurons expressed Syp:mCherry in intact, Cx, and Cx primed males, respectively; Figure 4, 100 ± 10% and 81 ± 6% of Pvl neurons expressed Syp:mCherry in diestrus and estrus females; Figure 5, 86 ± 8% of Pvl neurons expressed DREADDq; Figure 6, 105 ± 8% and 109 ± 5% of Pvl neurons expressed eNpHR3.0 and EYFP; Figure 7A–C, 108 ± 16% and 108 ± 8% of Pvl neurons expressed Syp:mCherry in vehicle or estrogen treated Ovx females). To quantify number of Syp:mCherry+ neurons (Figure 7G–I), we enumerated the number of such cells in the VMHvl on the control (EGFP) side as described above in the central three sections through this region and then expressed the number of Syp:mCherry+ neurons on the experimental (Cre:EGFP) side as a percent of the control side (100 ± 26% and 140 ± 35% of VMHvl neurons expressed Syp:mCherry on control and experimental side; p = 0.37).

Tracing studies—Except for experiments of Figure 4, we performed Ovx on all females at the time of viral delivery and analyzed presynaptic termini 2-3 weeks following viral delivery. For analyzing projections of Pvl neurons in males, males were left intact or Cx at the time of viral delivery as described in Figure 3. Mice were perfused 4-6 hours following last injection of hormone or vehicle for all experiments except for those described in Figure 4.

We did not perform Ovx on females used in experiments described in Figure 4. Two weeks following viral delivery, we examined the estrous stage of these females on a daily basis using vaginal cytology as described before (Xu et al., 2012; Yang et al., 2013). In brief, the vaginal canal was flushed with 15 μL of PBS, and this solution was spread on a glass slide, coverslipped, and imaged immediately under brightfield illumination. All females were allowed to undergo one complete estrous cycle prior to being perfused for histological analysis. Collection of vaginal cytology can occasionally induce a state of persistent diestrus, and these females were excluded from further analysis. We perfused females in diestrus, proestrus, and estrus to analyze projection termini of Pvl neurons. The density of presynaptic termini (quantification procedures described below) in the AVPV was similar in proestrus and estrus females and significantly greater than in diestrus females. Female mice are receptive during proestrus and estrus, and we therefore combined data from proestrus and estrus females for presentation (Figure 4).

To analyze projection termini of Pvl neurons, sections containing AVPV, POA, and PAG were collected, immunolabeled for mCherry or mRuby, and confocaled using a 63x objective, with image stacks containing 3 optical sections at 4 μm intervals. This imaging protocol was chosen to rigorously image individual presynaptic termini. Sections containing VMHvl were confocaled using a 20x objective, with image stacks containing 5 optical sections at 10 μm intervals. The number of presynaptic termini was enumerated using Image J software (Analyze Particle plugin) and divided by the area imaged to obtain the density of these termini in any given region. This estimate of the density of presynaptic termini was then normalized by the number of mCherry+ Pvl neurons to correct for subtle variations in infection in each animal. This normalized density of presynaptic termini is represented as a fraction of control (Ovx and vehicle administration in Figures 3D–F, 7C, S3D–F, S7A,B; intact male in Figure 3I–K; Diestrus female in Figure 4C–E; $PR^{PL/PL}$ in Figure 7F; EGFP in Figures 7I and S7 K,L)

We quantified the area occupied by axons of Pvl neurons by analyzing mGFP expression 2-3 weeks following viral delivery. Sections containing AVPV, POA, and PAG were confocaled using a 63x objective, with image stacks containing 9 optical sections at 1 μm intervals. Background signal intensity (obtained from areas containing no mGFP+ fibers or cell bodies) was subtracted from these stacks. The area occupied by mGFP+ fibers was then estimated using Image J software (Measurement plugin) by quantifying area containing pixels with intensity value >1. This areal estimate was then normalized by the number of mGFP+ Pvl neurons to correct for subtle variations in infection in each animal. This normalized area is represented as a fraction of control (Ovx and vehicle administration in Figure S3G–I).

To quantify vGlut2 and Syp:mCherry co-labeling, we expressed virally encoded Cre-dependent Syp:mCherry in Pvl neurons as described above and immunolabeled for mCherry and vGlut2. We then enumerated ≥250 mCherry+ presynaptic termini in 3 histological sections (65 μm each in the coronal plane) spanning the AVPV that had been imaged at 63x on a confocal microscope. These mCherry+ termini were then examined for vGlut2 expression.

To achieve maximal ablation of Pvl neurons following delivery of AAV-flex-taCasp3-TEVp, we waited for four weeks {a timepoint established by (Yang et al., 2013)}. We then injected 0.3 μL of the retrograde tracer CTB (conjugated to Alexa Fluor 555) into the AVPV. Mice were perfused 5 days after CTB injection. The middle three sections through the VMHvl were confocaled using a 20x objective, with image stacks containing 5 optical sections at 10 μm intervals. The number of CTB+ cells in the VMHvl was quantified using Photoshop (manual counting) and ImageJ software (Analyze Particle plugin for automated enumeration). CTB+ neuron counts in PR^{Cre} females are represented as a fraction of the CTB+ neuron counts in the VMHvl of WT females (Figure S7).

To examine the role of Esr1 in modulating presynaptic termini of Pvl neurons, mice were primed and perfused for histological analysis 2 weeks following lentiviral injections. The density of presynaptic termini was quantified as described above. To confirm Esr1 deletion, we immunolabeled for Esr1, confocaled and enumerated as described above for CTB+ cells.

Electrophysiology—Brain slices (300 μm) were obtained using standard techniques (Wu et al., 2015). Briefly, animals were anesthetized with isoflurane and decapitated. The brain was exposed and chilled with ice-cold artificial CSF (ACSF) containing 125 mM NaCl, 2.5 mM KCl, 2 mM $CaCl_2$, 1.25 mM NaH_2PO_4, 1 mM $MgCl_2$, 25 mM $NaHCO_3$, and 15 mM D-glucose. ACSF was saturated with 95% O_2 and 5% CO_2. Osmolarity was adjusted to 300-305 mOsm. Coronal brain slices containing AVPV were prepared with a vibrating microtome (Leica VT1200 S, Germany) and left to recover in ACSF for 30 min at 34°C and then at room temperature for an additional 30 min before recording. AVPV neurons were visualized under infrared illumination using an Olympus BX51WI microscope equipped with DIC, a water-immersion objective (40× NA 0.8), and a CMOS camera (Hamamatsu Photonics). Whole-cell voltage-clamp recording was performed at room temperature with borosilicate glass microelectrodes (3-5 MΩ) filled with a Cs^+-based low Cl^- internal solution (126 mM $CsMeSO_3$, 8 mM NaCl, 10 mM HEPES, 2.9 mM QX-314, 8 mM Na_2-Phosphocreatine, 0.3 mM GTP-Na, 4 mM ATP-Mg, 0.1 mM $CaCl_2$, 1 mM EGTA; pH 7.2-7.3; osmolarity 285-290 mOsm). The access resistance was < 25MΩ (no compensation), and the data were discarded if the access resistance changed more than 20% during recording. For recording of miniature EPSC (mEPSC), TTX (1 μM) was included, neurons were held at membrane potential of the Cl^- reversal potential (−70 mV, liquid junction potential not corrected). To examine optogenetically-evoked EPSC (oEPSC), we targeted AAV2-EF1a-DIO-ChR2:mCherry to the VMHvl of PR^{Cre} mice, and prepared coronal brain slices 8-10 weeks after viral delivery. To evoke oEPSC, a brief (0.2 ms) blue light stimulation was applied using a 450 nm laser (OptoEngine, USA). The laser was focused at the back aperture of the objective to achieve full field illumination. In order to measure the peak amplitude of oEPSCs, we gradually increased the blue light intensity till the oEPSC amplitude plateaued (< 10% increase with 2-3 folds increase in laser intensity). Recordings were obtained with a Multiclamp 700B amplifier (Molecular Devices) using the WinWCP software (University of Strathclyde, UK). Signals were filtered at 2 kHz, digitized at 10 kHz (NI PCIe-6259, National Instruments), and analyzed offline using Clampfit 10.0 (Molecular Devices) and Mini Analysis Program (Synaptosoft).

QUANTIFICATION AND STATISTICAL ANALYSIS

All data were analyzed blind to relevant variables including estrous cycle, hormonal treatment, genotype (mice and virus), CNO administration, light illumination conditions. Statistical analysis was performed using GraphPad PRISM (GraphPad Software). To compare categorical data, Fisher's exact test was performed from a 2x2 contingency table (Figures 2E,J,O, S2E,J,P,W, 6F,J, S6E,J). For non-categorical data, we first analyzed if the data values came from a normal distribution with D'Agostino-Pearson omnibus normality test. In experiments with paired samples, we used a paired t test (Figures S1B,D,F,H,J,L,N,P, 2G,H,L–N, S2B–D, H,M–O,T–V, 6C–E,G–I, S6B–D,G–I, 7I, S7J–L) and Wilcoxon matched-pairs signed rank test (Figures 2B–D,I, S2G,I) for parametric and non-parametric data, respectively. In all other experiments, we used a t test (Figures 1C,D, S2L, 3E,F, S3D–I, 4D,E, S4A,B, 5F,G, 7C,F, S7A,D,E,H), t test with Welch's correction for unequal standard deviation (Figures S2S, 3D, 5J), or ANOVA (Figures 1I,K,O, 3I–K, 5C, S5E) for parametric data and a Kruskal-Wallis test (Figure S1Q) or Mann-Whitney test (Figures 4C, S7B) for non-parametric data. All sample sizes and definitions as well precision measures (mean, SEM) are provided in figure legends.

DATA AND CODE AVAILABILITY

The published article includes all datasets generated and analyzed during the study. No new code was used in this study.

Supplementary Material

Refer to Web version on PubMed Central for supplementary material.

ACKNOWLEDGEMENTS

We thank Liqun Luo for reagents and Liqun Luo and members of the Shah lab for discussions or comments on the manuscript. This work is supported by grants to JD (R01NS091144 and GG Gift Fund) and NMS (R01NS049488; R01NS083872).

REFERENCES

Adler N, Pfaff D, and Goy RW (1985). Handbook of Behavioral Neurobiology, Volume 7, Reproduction (New York: Plenum Press).

Allen E (1922). The oestrous cycle in the mouse. Am. J. Anat 30, 297–371.

Arnold AP (2009). The organizational-activational hypothesis as the foundation for a unified theory of sexual differentiation of all mammalian tissues. Horm. Behav 55, 570–578. [PubMed: 19446073]

Bailey CH, and Kandel ER (2008). Synaptic remodeling, synaptic growth and the storage of long-term memory in Aplysia. Prog. Brain Res 169, 179–198. [PubMed: 18394474]

Balthazart J, and Ball GF (2016). Endocrine and social regulation of adult neurogenesis in songbirds. Front. Neuroendocrinol 41, 3–22. [PubMed: 26996818]

Barfield RJ, and Chen JJ (1977). Activation of estrous behavior in ovariectomized rats by intracerebral implants of estradiol benzoate. Endocrinology 101, 1716–1725. [PubMed: 338289]

Baroncini M, Jissendi P, Catteau-Jonard S, Dewailly D, Pruvo J-P, Francke J-P, and Prevot V (2010). Sex steroid hormones-related structural plasticity in the human hypothalamus. Neuroimage 50, 428–433. [PubMed: 19969095]

Bayless DW, Yang T, Mason MM, Susanto AAT, Lobdell A, and Shah NM (2019). Limbic Neurons Shape Sex Recognition and Social Behavior in Sexually Naive Males. Cell 176, 1190–1205.e20. [PubMed: 30712868]

Beier KT, Steinberg EE, DeLoach KE, Xie S, Miyamichi K, Schwarz L, Gao XJ, Kremer EJ, Malenka RC, and Luo L (2015). Circuit Architecture of VTA Dopamine Neurons Revealed by Systematic Input-Output Mapping. Cell 162, 622–634. [PubMed: 26232228]

Blaustein JD (2008). Neuroendocrine regulation of feminine sexual behavior: lessons from rodent models and thoughts about humans. Annu. Rev. Psychol 59, 93–118. [PubMed: 17678443]

Blaustein JD, Tetel MJ, Ricciardi KH, Delville Y, and Turcotte JC (1994). Hypothalamic ovarian steroid hormone-sensitive neurons involved in female sexual behavior. Psychoneuroendocrinology 19, 505–516. [PubMed: 7938350]

Brenner RM, and West NB (1975). Hormonal regulation of the reproductive tract in female mammals. Annu. Rev. Physiol 37, 273–302. [PubMed: 164819]

Bronson FH (1979). The reproductive ecology of the house mouse. Q. Rev. Biol 54, 265–299. [PubMed: 390600]

Cao P, Maximov A, and Südhof TC (2011). Activity-Dependent IGF-1 Exocytosis Is Controlled by the Ca2+-Sensor Synaptotagmin-10. Cell 145, 300–311. [PubMed: 21496647]

Chan H, Prescott M, Ong Z, Herde MK, Herbison AE, and Campbell RE (2011). Dendritic spine plasticity in gonadatropin-releasing hormone (GnRH) neurons activated at the time of the preovulatory surge. Endocrinology 152, 4906–4914. [PubMed: 21933865]

Chen T-W, Wardill TJ, Sun Y, Pulver SR, Renninger SL, Baohan A, Schreiter ER, Kerr RA, Orger MB, Jayaraman V, et al. (2013). Ultrasensitive fluorescent proteins for imaging neuronal activity. Nature 499, 295–300. [PubMed: 23868258]

Chen Y, Lin Y-C, Kuo T-W, and Knight ZA (2015). Sensory detection of food rapidly modulates arcuate feeding circuits. Cell 160, 829–841. [PubMed: 25703096]

Clasadonte J, and Prevot V (2018). The special relationship: glia-neuron interactions in the neuroendocrine hypothalamus. Nat. Rev. Endocrinol 14, 25–44. [PubMed: 29076504]

Cooke BM, and Woolley CS (2005). Gonadal hormone modulation of dendrites in the mammalian CNS. J. Neurobiol 64, 34–46. [PubMed: 15884004]

Cui G, Jun SB, Jin X, Pham MD, Vogel SS, Lovinger DM, and Costa RM (2013). Concurrent activation of striatal direct and indirect pathways during action initiation. Nature 494, 238–242. [PubMed: 23354054]

Davis PG, Krieger MS, Barfield RJ, McEwen BS, and Pfaff DW (1982). The site of action of intrahypothalamic estrogen implants in feminine sexual behavior: an autoradiographic analysis. Endocrinology 111, 1581–1586. [PubMed: 7128527]

DeLeon DD, Zelinski-Wooten MB, and Barkley MS (1990). Hormonal basis of variation in oestrous cyclicity in selected strains of mice. J. Reprod. Fertil 89, 117–126. [PubMed: 2374113]

Dey S, Chamero P, Pru JK, Chien M-S, Ibarra-Soria X, Spencer KR, Logan DW, Matsunami H, Peluso JJ, and Stowers L (2015). Cyclic Regulation of Sensory Perception by a Female Hormone Alters Behavior. Cell 161, 1334–1344. [PubMed: 26046438]

Feng Y, Manka D, Wagner K-U, and Khan SA (2007). Estrogen receptor-alpha expression in the mammary epithelium is required for ductal and alveolar morphogenesis in mice. Proc. Natl. Acad. Sci. U. S. A 104, 14718–14723. [PubMed: 17785410]

Fenno L, Yizhar O, and Deisseroth K (2011). The development and application of optogenetics. Annu. Rev. Neurosci 34, 389–412. [PubMed: 21692661]

Fernald RD (1995). Social control of cell size: males and females are different. Prog. Brain Res 105, 171–177. [PubMed: 7568874]

Frankfurt M, Gould E, Woolley CS, and McEwen BS (1990). Gonadal steroids modify dendritic spine density in ventromedial hypothalamic neurons: a Golgi study in the adult rat. Neuroendocrinology 51, 530–535. [PubMed: 2112730]

Goy RW, and Phoenix CH (1963). Hypothalamic regulation of female sexual behaviour; establishment of behavioural oestrus in spayed guinea-pigs following hypothalamic lesions. J. Reprod. Fertil 5, 23–40. [PubMed: 13949643]

Gradinaru V, Zhang F, Ramakrishnan C, Mattis J, Prakash R, Diester I, Goshen I, Thompson KR, and Deisseroth K (2010). Molecular and cellular approaches for diversifying and extending optogenetics. Cell 141, 154–165. [PubMed: 20303157]

Gunaydin LA, Grosenick L, Finkelstein JC, Kauvar IV, Fenno LE, Adhikari A, Lammel S, Mirzabekov JJ, Airan RD, Zalocusky KA, et al. (2014). Natural neural projection dynamics underlying social behavior. Cell 157, 1535–1551. [PubMed: 24949967]

Hart MP, and Hobert O (2018). Neurexin controls plasticity of a mature, sexually dimorphic neuron. Nature 553, 165–170. [PubMed: 29323291]

Harvey W, and Guyton AC (1989). The Works of William Harvey (Philadelphia: University of Pennsylvania Press).

Hashikawa K, Hashikawa Y, Tremblay R, Zhang J, Feng JE, Sabol A, Piper WT, Lee H, Rudy B, and Lin D (2017). Esr1+ cells in the ventromedial hypothalamus control female aggression. Nat. Neurosci 20, 1580–1590. [PubMed: 28920934]

Hellier V, Brock O, Candlish M, Desroziers E, Aoki M, Mayer C, Piet R, Herbison A, Colledge WH, Prévot V, et al. (2018). Female sexual behavior in mice is controlled by kisspeptin neurons. Nat. Commun 9, 400. [PubMed: 29374161]

Hu H, Real E, Takamiya K, Kang M-G, Ledoux J, Huganir RL, and Malinow R (2007). Emotion enhances learning via norepinephrine regulation of AMPA-receptor trafficking. Cell 131, 160–173. [PubMed: 17923095]

Ishii KK, Osakada T, Mori H, Miyasaka N, Yoshihara Y, Miyamichi K, and Touhara K (2017). A Labeled-Line Neural Circuit for Pheromone-Mediated Sexual Behaviors in Mice. Neuron 95, 123–137.e8. [PubMed: 28648498]

Kauer JA, and Malenka RC (2007). Synaptic plasticity and addiction. Nat. Rev. Neurosci 8, 844–858. [PubMed: 17948030]

Kendrick AM, Rand MS, and Crews D (1995). Electrolytic lesions to the ventromedial hypothalamus abolish receptivity in female whiptail lizards, Cnemidophorus uniparens. Brain Res. 680, 226–228. [PubMed: 7663980]

Konishi M (1989). Birdsong for neurobiologists. Neuron 3, 541–549. [PubMed: 2701843]

Konishi M, and Akutagawa E (1985). Neuronal growth, atrophy and death in a sexually dimorphic song nucleus in the zebra finch brain. Nature 315, 145–147. [PubMed: 3990816]

Kudwa AE, Bodo C, Gustafsson J-A, and Rissman EF (2005). A previously uncharacterized role for estrogen receptor beta: defeminization of male brain and behavior. Proc. Natl. Acad. Sci. U. S. A 102, 4608–4612. [PubMed: 15761056]

Kudwa AE, Michopoulos V, Gatewood JD, and Rissman EF (2006). Roles of estrogen receptors alpha and beta in differentiation of mouse sexual behavior. Neuroscience 138, 921–928. [PubMed: 16338079]

Lee H, Kim D-W, Remedios R, Anthony TE, Chang A, Madisen L, Zeng H, and Anderson DJ (2014). Scalable control of mounting and attack by Esr1+ neurons in the ventromedial hypothalamus. Nature 509, 627–632. [PubMed: 24739975]

Leedy MG, and Hart BL (1985). Female and male sexual responses in female cats with ventromedial hypothalamic lesions. Behav. Neurosci 99, 936–941. [PubMed: 3843309]

Lindburg DG, Czekala NM, and Swaisgood RR (2001). Hormonal and behavioral relationships during estrus in the giant panda. Zoo Biol. 20, 537–543.

Liu Q, Tabuchi M, Liu S, Kodama L, Horiuchi W, Daniels J, Chiu L, Baldoni D, and Wu MN (2017). Branch-specific plasticity of a bifunctional dopamine circuit encodes protein hunger. Science 356, 534–539. [PubMed: 28473588]

Lo L, Yao S, Kim D-W, Cetin A, Harris J, Zeng H, Anderson DJ, and Weissbourd B (2019). Connectional architecture of a mouse hypothalamic circuit node controlling social behavior. Proc. Natl. Acad. Sci. U. S. A 116, 7503–7512. [PubMed: 30898882]

Lubahn DB, Moyer JS, Golding TS, Couse JF, Korach KS, and Smithies O (1993). Alteration of reproductive function but not prenatal sexual development after insertional disruption of the mouse estrogen receptor gene. Proc. Natl. Acad. Sci. U. S. A 90, 11162–11166. [PubMed: 8248223]

Luine V, and Frankfurt M (2013). Interactions between estradiol, BDNF and dendritic spines in promoting memory. Neuroscience 239, 34–45. [PubMed: 23079626]

Lydon JP, DeMayo FJ, Funk CR, Mani SK, Hughes AR, Montgomery CA Jr, Shyamala G, Conneely OM, and O'Malley BW (1995). Mice lacking progesterone receptor exhibit pleiotropic reproductive abnormalities. Genes Dev. 9, 2266–2278. [PubMed: 7557380]

Maguire J, and Mody I (2009). Steroid hormone fluctuations and GABA(A)R plasticity. Psychoneuroendocrinology 34 Suppl 1, S84–90. [PubMed: 19632051]

Maruska KP, and Fernald RD (2013). Social regulation of male reproductive plasticity in an African cichlid fish. Integr. Comp. Biol 53, 938–950. [PubMed: 23613320]

Mathews D, Donovan KM, Hollingsworth EM, Hutson VB, and Overstreet CT (1983). Permanent deficits in lordosis behavior in female rats with lesions of the ventromedial nucleus of the hypothalamus. Exp. Neurol 79, 714–719. [PubMed: 6825760]

McHenry JA, Otis JM, Rossi MA, Robinson JE, Kosyk O, Miller NW, McElligott ZA, Budygin EA, Rubinow DR, and Stuber GD (2017). Hormonal gain control of a medial preoptic area social reward circuit. Nat. Neurosci 20, 449–458. [PubMed: 28135243]

Montagnese C, Poulain DA, and Theodosis DT (1990). Influence of ovarian steroids on the ultrastructural plasticity of the adult rat supraoptic nucleus induced by central administration of oxytocin. J. Neuroendocrinol 2, 225–231. [PubMed: 19210388]

Morris JA, Jordan CL, and Breedlove SM (2004). Sexual differentiation of the vertebrate nervous system. Nat. Neurosci 7, 1034–1039. [PubMed: 15452574]

Musatov S, Chen W, Pfaff DW, Kaplitt MG, and Ogawa S (2006). RNAi-mediated silencing of estrogen receptor {alpha} in the ventromedial nucleus of hypothalamus abolishes female sexual behaviors. Proc. Natl. Acad. Sci. U. S. A 103, 10456–10460. [PubMed: 16803960]

Mysore SP, Tai C-Y, and Schuman EM (2008). N-cadherin, spine dynamics, and synaptic function. Front. Neurosci 2, 168–175. [PubMed: 19225589]

Nelson JF, Felicio LS, Osterburg HH, and Finch CE (1992). Differential contributions of ovarian and extraovarian factors to age-related reductions in plasma estradiol and progesterone during the estrous cycle of C57BL/6J mice. Endocrinology 130, 805–810. [PubMed: 1733727]

Ng L, Bernard A, Lau C, Overly CC, Dong H-W, Kuan C, Pathak S, Sunkin SM, Dang C, Bohland JW, et al. (2009). An anatomic gene expression atlas of the adult mouse brain. Nat. Neurosci 12, 356–362. [PubMed: 19219037]

Nicoll RA (2017). A Brief History of Long-Term Potentiation. Neuron 93, 281–290. [PubMed: 28103477]

Osakada T, Ishii KK, Mori H, Eguchi R, Ferrero DM, Yoshihara Y, Liberles SD, Miyamichi K, and Touhara K (2018). Sexual rejection via a vomeronasal receptor-triggered limbic circuit. Nat. Commun 9, 4463. [PubMed: 30367054]

Pfaff DW, and Sakuma Y (1979). Deficit in the lordosis reflex of female rats caused by lesions in the ventromedial nucleus of the hypothalamus. J. Physiol 288, 203–210. [PubMed: 469716]

Pleim ET, Brown TJ, MacLusky NJ, Etgen AM, and Barfield RJ (1989). Dilute estradiol implants and progestin receptor induction in the ventromedial nucleus of the hypothalamus: correlation with receptive behavior in female rats. Endocrinology 124, 1807–1812. [PubMed: 2924724]

Pletzer B, Kronbichler M, Aichhorn M, Bergmann J, Ladurner G, and Kerschbaum HH (2010). Menstrual cycle and hormonal contraceptive use modulate human brain structure. Brain Res. 1348, 55–62. [PubMed: 20550945]

Ray RS, Corcoran AE, Brust RD, Kim JC, Richerson GB, Nattie E, and Dymecki SM (2011). Impaired respiratory and body temperature control upon acute serotonergic neuron inhibition. Science 333, 637–642. [PubMed: 21798952]

Reisert I, Han V, Lieth E, Toran-Allerand D, Pilgrim C, and Lauder J (1987). Sex steroids promote neurite growth in mesencephalic tyrosine hydroxylase immunoreactive neurons in vitro. Int. J. Dev. Neurosci. Off. J. Int. Soc. Dev. Neurosci 5, 91–98.

Ring JR (1944). The estrogen-progesterone induction of sexual receptivity in the spayed female mouse. Endocrinology 34, 269–275.

Rissman EF, Early AH, Taylor JA, Korach KS, and Lubahn DB (1997). Estrogen receptors are essential for female sexual receptivity. Endocrinology 138, 507–510. [PubMed: 8977441]

Robarts DW, and Baum MJ (2007). Ventromedial hypothalamic nucleus lesions disrupt olfactory mate recognition and receptivity in female ferrets. Horm. Behav 51, 104–113. [PubMed: 17011561]

Roth BL (2016). DREADDs for Neuroscientists. Neuron 89, 683–694. [PubMed: 26889809]

Rubin BS, and Barfield RJ (1980). Priming of estrous responsiveness by implants of 17 beta-estradiol in the ventromedial hypothalamic nucleus of female rats. Endocrinology 106, 504–509. [PubMed: 6986255]

Sasaki K, Suzuki M, Mieda M, Tsujino N, Roth B, and Sakurai T (2011). Pharmacogenetic modulation of orexin neurons alters sleep/wakefulness states in mice. PloS One 6, e20360. [PubMed: 21647372]

Scott N, Prigge M, Yizhar O, and Kimchi T (2015). A sexually dimorphic hypothalamic circuit controls maternal care and oxytocin secretion. Nature 525, 519–522. [PubMed: 26375004]

Simerly RB (2002). Wired for reproduction: organization and development of sexually dimorphic circuits in the mammalian forebrain. Annu. Rev. Neurosci 25, 507–536. [PubMed: 12052919]

Sternson SM, and Roth BL (2014). Chemogenetic tools to interrogate brain functions. Annu. Rev. Neurosci 37, 387–407. [PubMed: 25002280]

Swaab D (2003). The ventromedial nucleus (VMN; nucleus of Cajal) In The Human Hypothalamus: Basic and Clinical Aspects Part I: Nuclei of the Human Hypothalamus, (Elsevier), pp. 239–242.

Tamamaki N, Yanagawa Y, Tomioka R, Miyazaki J-I, Obata K, and Kaneko T (2003). Green fluorescent protein expression and colocalization with calretinin, parvalbumin, and somatostatin in the GAD67-GFP knock-in mouse. J. Comp. Neurol 467, 60–79. [PubMed: 14574680]

Thompson ML, and Edwards DA (1971). Experiential and strain determinants of the estrogen-progesterone induction of sexual receptivity in spayed female mice. Horm. Behav 2, 299–305.

Toran-Allerand CD (1976). Sex steroids and the development of the newborn mouse hypothalamus and preoptic area in vitro: implications for sexual differentiation. Brain Res. 106, 407–412. [PubMed: 1276881]

Tuscher JJ, Luine V, Frankfurt M, and Frick KM (2016). Estradiol-Mediated Spine Changes in the Dorsal Hippocampus and Medial Prefrontal Cortex of Ovariectomized Female Mice Depend on ERK and mTOR Activation in the Dorsal Hippocampus. J. Neurosci. Off. J. Soc. Neurosci 36, 1483–1489.

Unger EK, Burke KJ, Yang CF, Bender KJ, Fuller PM, and Shah NM (2015). Medial amygdalar aromatase neurons regulate aggression in both sexes. Cell Rep. 10, 453–462. [PubMed: 25620703]

Wang S, Zhu J, and Xu T (2018). 17β-estradiol (E2) promotes growth and stability of new dendritic spines via estrogen receptor β pathway in intact mouse cortex. Brain Res. Bull 137, 241–248. [PubMed: 29288734]

Woolley CS, Gould E, Frankfurt M, and McEwen BS (1990). Naturally occurring fluctuation in dendritic spine density on adult hippocampal pyramidal neurons. J. Neurosci. Off. J. Soc. Neurosci 10, 4035–4039.

Wu MV, Manoli DS, Fraser EJ, Coats JK, Tollkuhn J, Honda S-I, Harada N, and Shah NM (2009). Estrogen masculinizes neural pathways and sex-specific behaviors. Cell 139, 61–72. [PubMed: 19804754]

Wu Y-W, Kim J-I, Tawfik VL, Lalchandani RR, Scherrer G, and Ding JB (2015). Input- and Cell-Type-Specific Endocannabinoid-Dependent LTD in the Striatum. Cell Rep. 10, 75–87. [PubMed: 25543142]

Xu X, Coats JK, Yang CF, Wang A, Ahmed OM, Alvarado M, Izumi T, and Shah NM (2012). Modular genetic control of sexually dimorphic behaviors. Cell 148, 596–607. [PubMed: 22304924]

Yang CF, and Shah NM (2014). Representing sex in the brain, one module at a time. Neuron 82, 261–278. [PubMed: 24742456]

Yang CF, Chiang MC, Gray DC, Prabhakaran M, Alvarado M, Juntti SA, Unger EK, Wells JA, and Shah NM (2013). Sexually dimorphic neurons in the ventromedial hypothalamus govern mating in both sexes and aggression in males. Cell 153, 896–909. [PubMed: 23663785]

Yang T, Yang CF, Chizari MD, Maheswaranathan N, Burke KJ, Borius M, Inoue S, Chiang MC, Bender KJ, Ganguli S, et al. (2017). Social Control of Hypothalamus-Mediated Male Aggression. Neuron 95, 955–970. e4. [PubMed: 28757304]

Highlights

- Projection termini of female Pvl neurons in AVPV increase during estrus
- Estrogen triggers the increase of Pvl projection termini in AVPV
- This structural plasticity increases functional connectivity between Pvl and AVPV
- Inhibiting projections from Pvl to AVPV in estrus inhibits female from mating

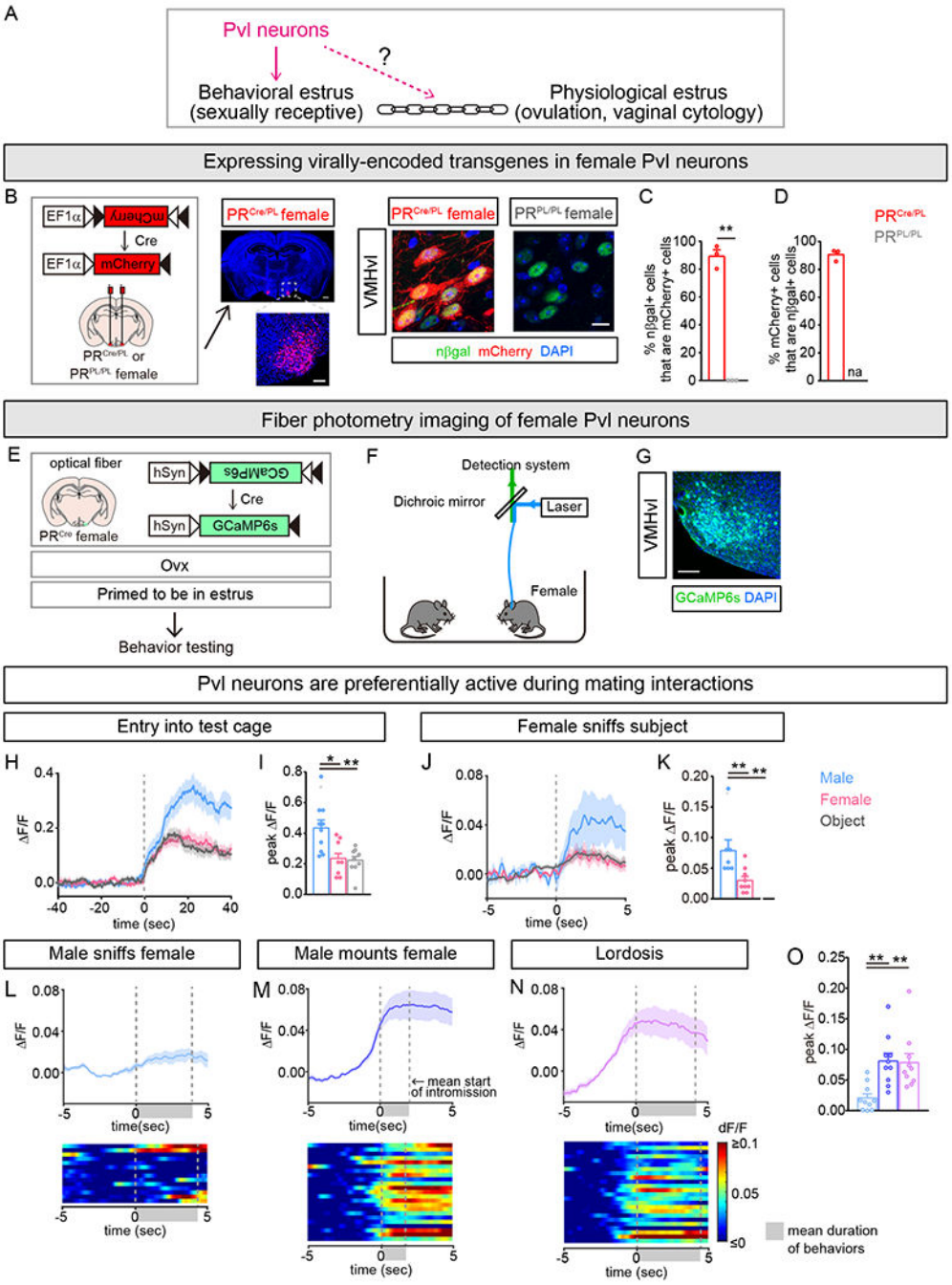

Figure 1: Female Pvl neurons are active during mating

(A) Pvl neurons are required for behavioral estrus, but whether Pvl neurons link behavioral estrus to physiological estrus is unknown.

(B) Strategy to express virally encoded, Cre-dependent transgenes in Pvl neurons of *PR*^{Cre} females. Middle: Coronal section shows that virally delivered mCherry is expressed in VMHvl but not surrounding regions [scale bars = 500μm and 100 μm (inset)]. Right: mCherry is expressed in *PR*$^{Cre/PL}$ but not *PR*$^{PL/PL}$ neurons (scale bar = 10 μm).

(C,D) Vast majority of mCherry+ or nβgal + Pvl neurons express nβgal or mCherry, respectively. Each dot in a bar graph in this and other Figures is data from one mouse.
(E-O) Fiber photometry imaging setup and activity of Pvl neurons in PR^{Cre} females upon insertion into test cage.
(G) Cre-dependent GCaMP6s expression in Pvl neurons (scale bar = 100 μm).
(H-K) Activation of Pvl neurons in PR^{Cre} female during interactions with WT male or primed female or wood block.
(H,J) Peri-event time plot (PETP) of GCaMP6s fluorescence around entry into test cage (H) and sniffing of resident animal or object (J). In this and Figure S1, dark line and lighter shading in same color indicates Mean and SEM of change in fluorescence for that group of mice.
(I,K) Pvl neurons are activated more upon entry into male cage (I) or upon sniffing male (K).
(L-O) Activity of Pvl neurons during mating with WT male. Data from interactions with male are from same animals and tests shown in (H-K).
(L-N) Top: PETP of GCaMP6s fluorescence around onset of male sniffing of female (L), male mounting (M), and lordosis (N). Bottom: Heat map of PETP, with individual events/row; data from a single female.
(O) Increased activation of Pvl neurons upon being mounted and during lordosis compared to being sniffed.
Mean ± SEM. n = 3 (C,D); n = 10 (H-O). *p<0.05, **p<0.01.
See also Figure S1, Table S1, and Movie S1.

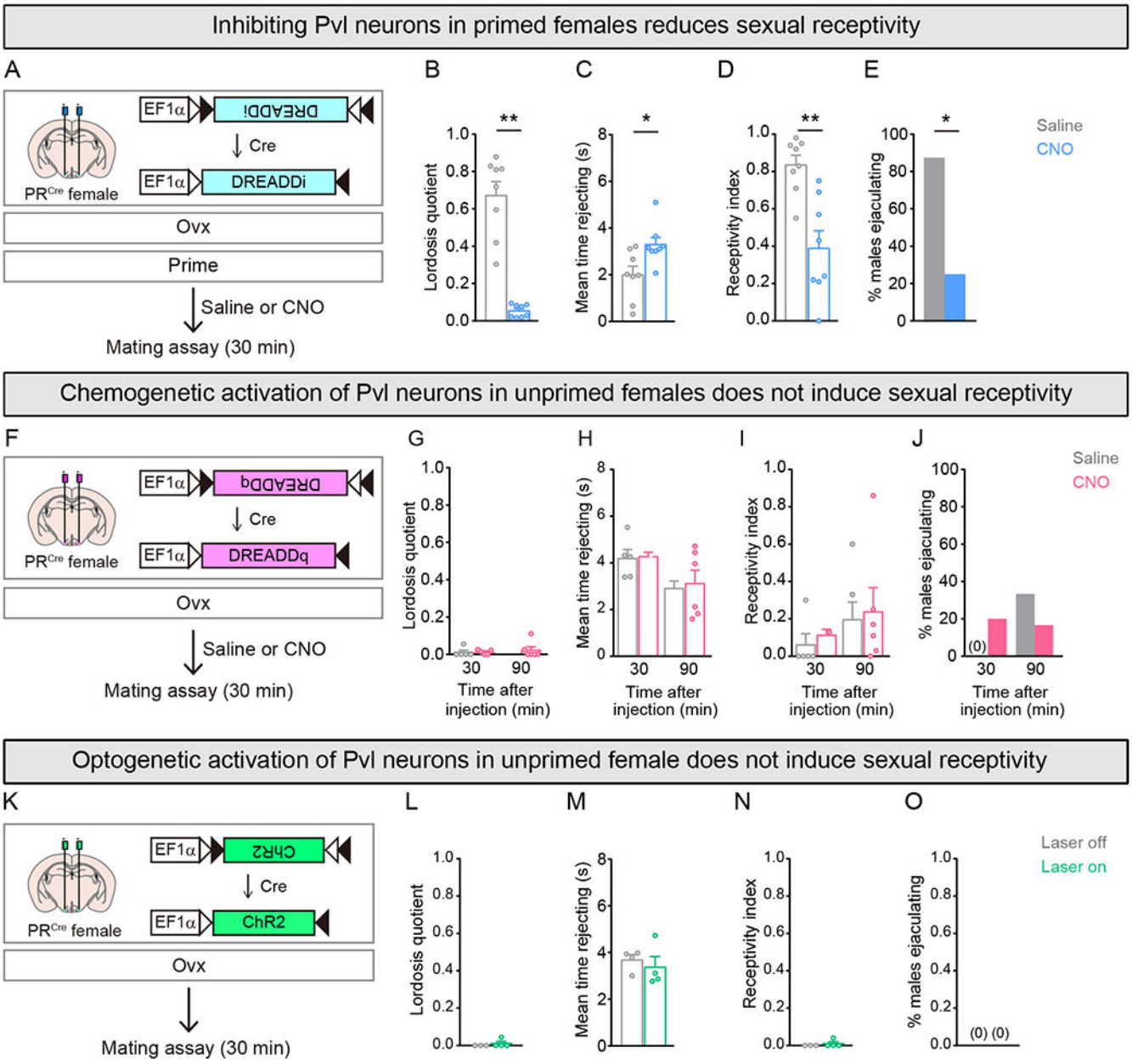

Figure 2: Activity of Pvl neurons is necessary but not sufficient for female sexual receptivity

(A-E) Chemogenetic inhibition of Pvl neurons with DREADDi.

(B-E) Primed females given CNO show diminution in sexual behavior and an increase in time rejecting males, leading to fewer males ejaculating during the test. Lordosis quotient = (# lordosis events)/(# mounts or intromissions); Receptivity index = (# intromissions)/(# mounts).

(F-J) Chemogenetic activation of Pvl neurons with DREADDq.

(G-J) No increase in sexual behavior of unprimed females 30 or 90 min after CNO.

(K-O) Optogenetic activation of Pvl neurons with ChR2.

(L-O) No increase in sexual behavior of unprimed females upon laser illumination of ChR2+ Pvl neurons.

Mean ± SEM. n = 8 (B-E); n = 5,6 (G-J); n = 4 (L-O). *p<0.05, **p<0.01.
See also Figure S2.

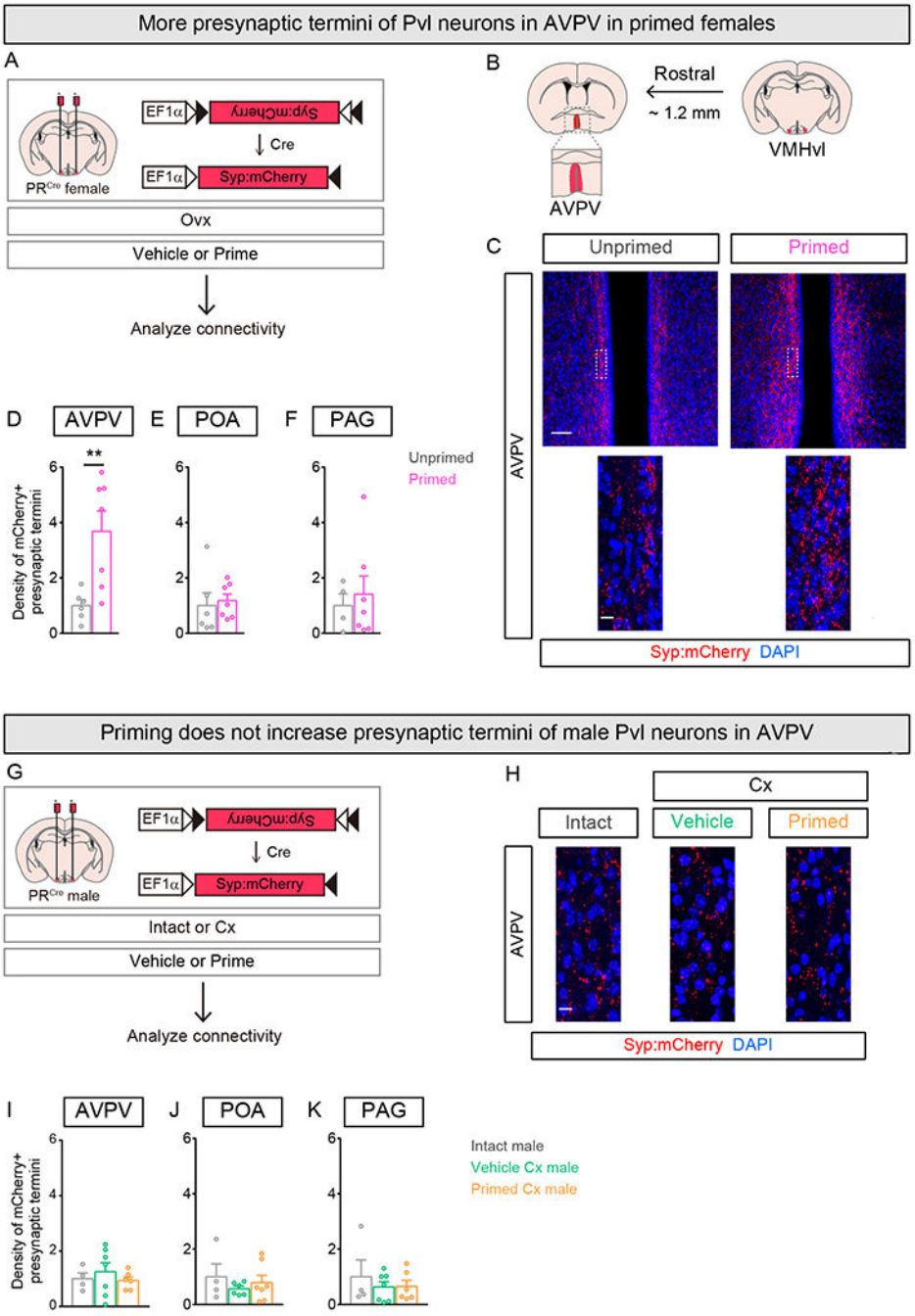

Figure 3. Ovarian sex hormones increase presynaptic termini of Pvl neurons in AVPV

(A-F) Labeling presynaptic termini of female Pvl neurons.

(B) Pvl neurons send ~1.2 mm projections to AVPV.

(C) More presynaptic termini (mCherry+) of Pvl neurons in AVPV visualized in primed females. Insets are higher magnification images of box outlined in top panels.

(D-F) Higher density of mCherry+ Pvl termini in AVPV but not other targets in primed females. Density of mCherry+ termini in this and other Figures has been normalized to

number of mCherry+ soma of Pvl neurons to account for subtle variability in infection of these cells. Change in density represented as fold change compared to unprimed female.
(G-K) Labeling presynaptic termini of male Pvl neurons.
(H) No visible difference in mCherry+ Pvl termini in AVPV in males under various hormonal regimes.
(I-K) No difference in density of mCherry+ Pvl presynaptic termini in AVPV or other targets. Change in density represented as fold change compared to intact male.
Mean ± SEM. n = 6 (Vehicle), 7 (Primed) (D-F); n = 4 (Intact), 7 (Vehicle Cx), 6 (Primed Cx) (I-K). Scale bars = 50 μm (C, top) and 10 μm (C insets, H). **p<0.01.
See also Figure S3.

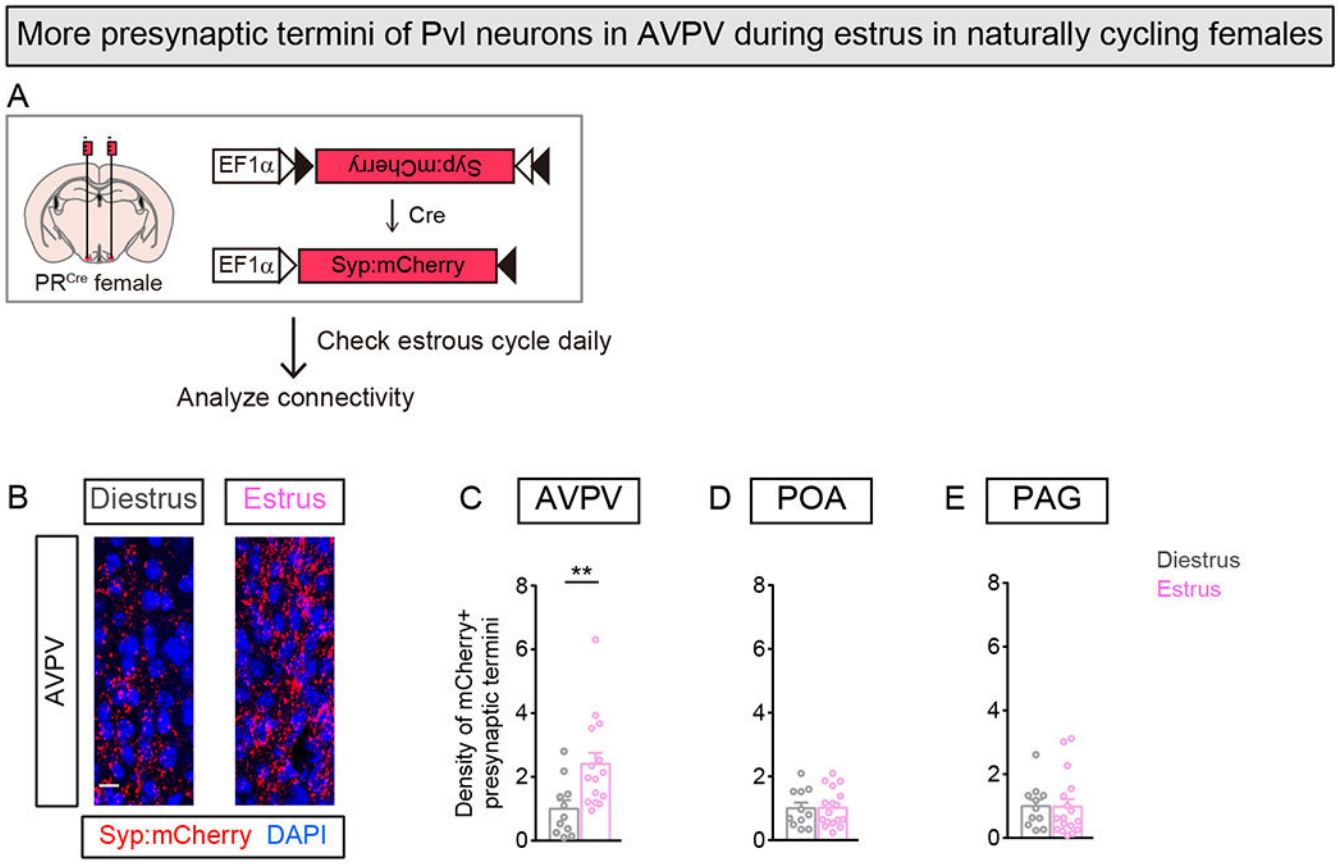

Figure 4. More Pvl projection termini in AVPV of naturally cycling estrus females

(A) Strategy to examine presynaptic termini of Pvl neurons in gonadally intact females.

(B) More mCherry+ Pvl termini in AVPV visualized in estrus female.

(C-E) Higher density of mCherry+ Pvl termini in AVPV, but not other target regions, in estrus female. Change in density represented as fold change compared to diestrus female. Mean ± SEM. n = 11 (Diestrus), 17 (Estrus) (C-E). Scale bar = 10μm. **p<0.01.

See also Figure S4.

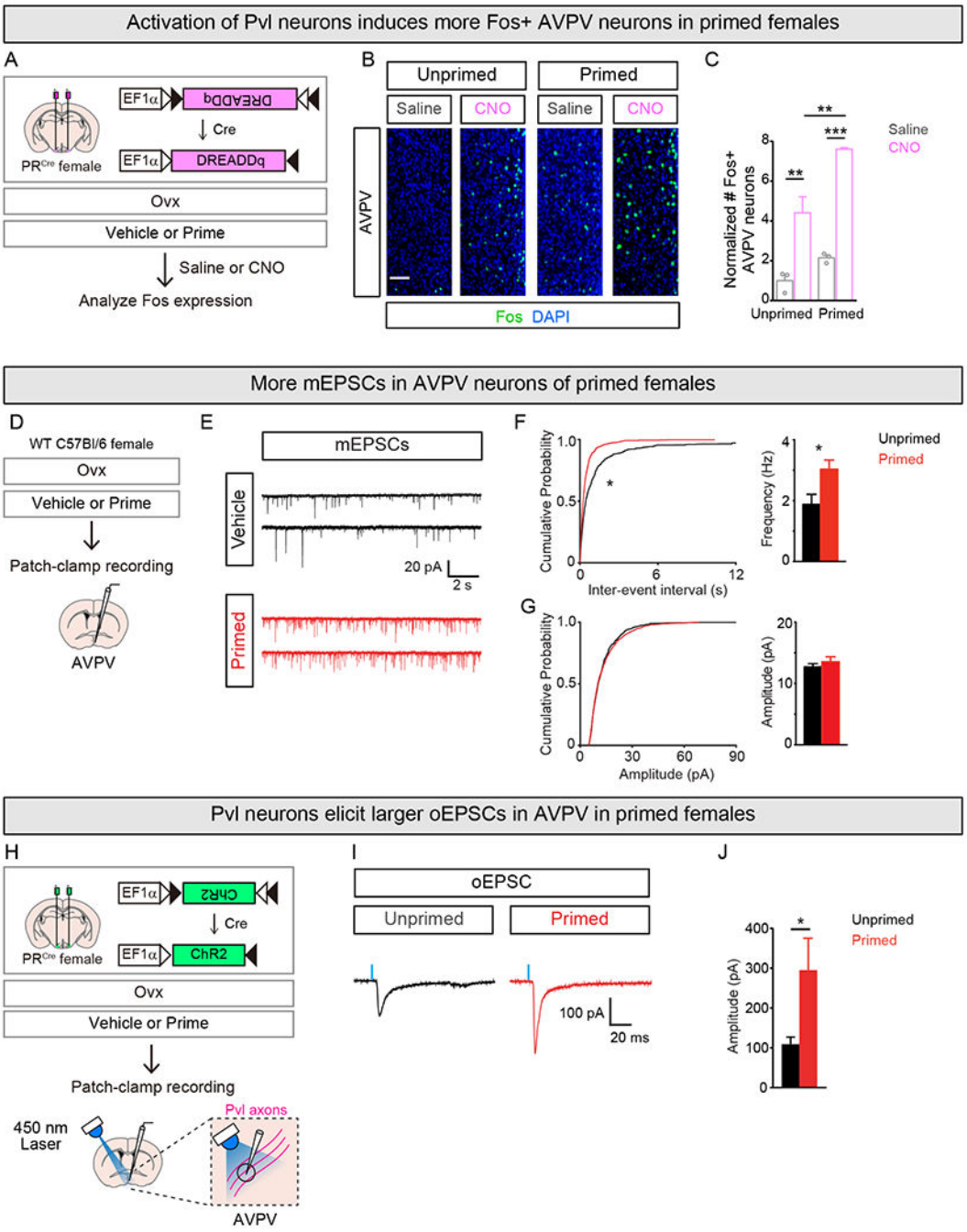

Figure 5. Ovarian sex hormones increase excitatory inputs to AVPV.

(A-C) Examining Fos induction in AVPV following activation of Pvl neurons.

(B,C) Activating Pvl neurons with CNO induces Fos in AVPV. More Fos+ AVPV neurons in primed than unprimed females. Counts of Fos+ AVPV neurons were normalized to number of DREADDq+ Pvl neurons for the respective experimental condition, and they are represented as fold change compared to unprimed female given saline.

(D-G) mEPSC recording with whole-cell voltage-clamp of AVPV neurons.

(E) Sample mEPSC traces recorded from AVPV neurons in unprimed and primed female.

(F) Shift in cumulative probability distribution of mEPSC inter-event interval (left) and higher mean mEPSC frequency (right) in primed than unprimed females.
(G) No difference in cumulative probability plots of mEPSC amplitudes (left) or mean amplitude (right) of mEPSCs between primed and unprimed females.
(H-J) Whole-cell voltage-clamp recording of oEPSCs in AVPV neurons elicited by 450nm laser illumination of ChR2+ Pvl axons.
(I) Sample oEPSC traces recorded from AVPV neurons primed and unprimed female.
(J) Larger peak amplitudes of oEPSCs in AVPV from primed compared to unprimed females.
Mean ± SEM. n = 3/condition (C); n = 24 (Unprimed), 25 (Primed) (F, G), 40 (Unprimed), 34 (Primed) (J) cells. Scale bar = 20μm. *p<0.05, **p<0.01, ***p<0.001.
See also Figure S5.

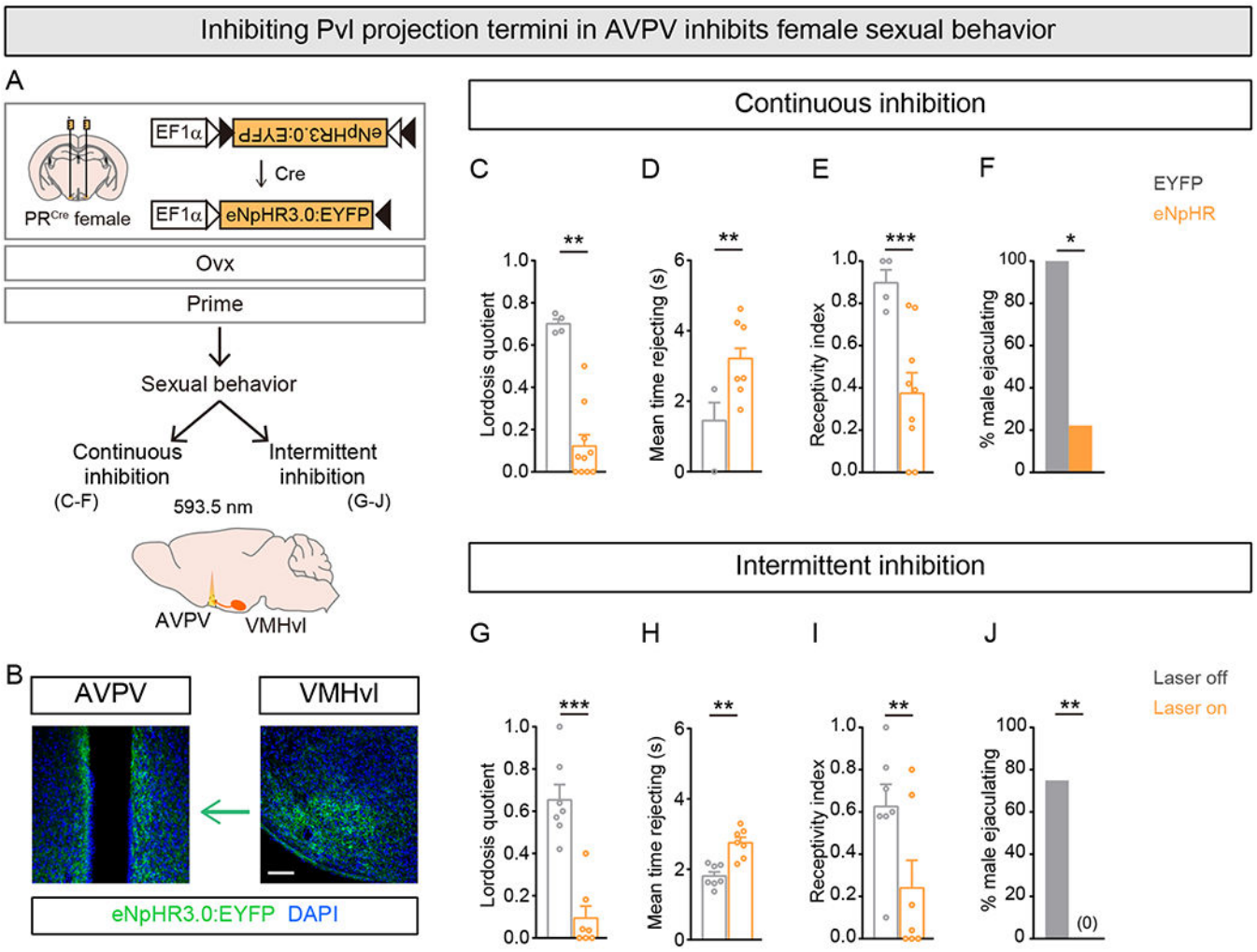

Figure 6. Inhibiting Pvl projection termini in AVPV reduces female sexual receptivity

(A) Experimental strategy to inhibit Pvl projection termini in AVPV in primed females.

(B) Coronal sections showing eNpHR3.0+ Pvl neurons in VMHvl and their projection termini in AVPV. For clarity, left VMHvl and left and right AVPV are shown.

(C-F) Continuous illumination of Pvl projection termini in AVPV reduces lordosis and increases rejection of male mating attempts, leading to fewer males ejaculating during the test.

(G-J) Intermittent illumination of Pvl projection termini in AVPV reduces lordosis and increases rejection of male mating attempts, leading to fewer males ejaculating when the laser is switched on.

Mean ± SEM. n = 4 (EYFP), 9 (eNpHR3.0) (C-F), 7/condition (G-J). Scale bar = 100 μm. *p<0.05, **p<0.01, ***p<0.001.

See also Figure S6 and Movie S2.

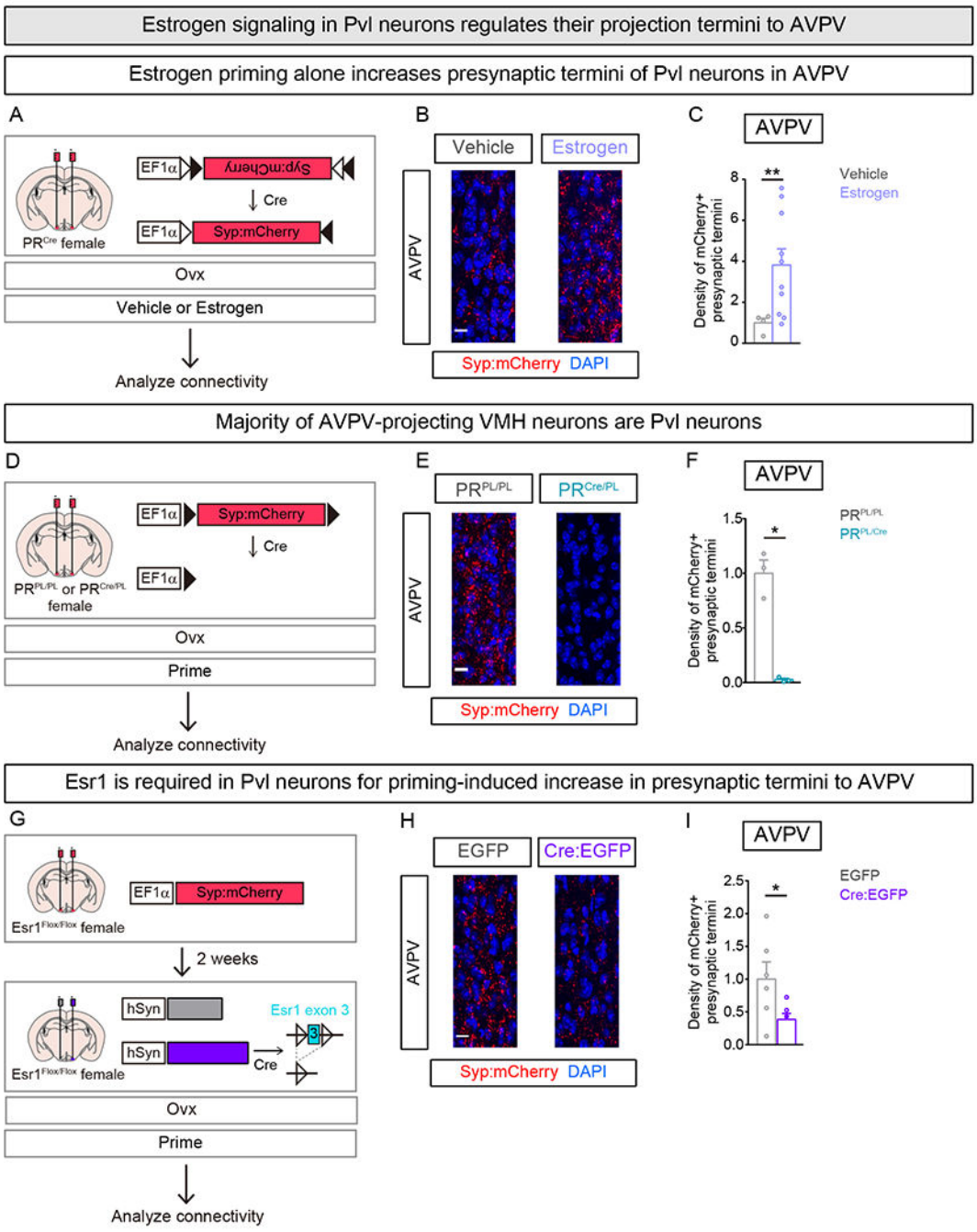

Figure 7. Estrogen signaling regulates plasticity of Pvl projections to AVPV

(A-C) Labeling presynaptic termini of Pvl neurons in vehicle or estrogen treated Ovx females.

(B) More mCherry+ presynaptic termini visualized in estrogen primed female AVPV.

(C) More mCherry+ presynaptic termini in estrogen primed female AVPV. Change in density represented as fold change compared to vehicle treated female.

(D-F) Labeling presynaptic termini of non-Pvl VMH neurons in female. Only Cre− neurons in VMH express Syp:mCherry.

(E) mCherry+ presynaptic termini in AVPV are apparent in $PR^{PL/PL}$ but not $PR^{Cre/PL}$ females.

(F) Lower density of mCherry+ presynaptic termini in AVPV of $PR^{Cre/PL}$ compared to $PR^{PL/PL}$ females. Change in density represented as fold change compared to $PR^{PL/PL}$ female.

(G-I) Examining role of Esr1 in plasticity of female VMH neuron projections to AVPV. AAV encoding constitutively expressed Syp:mCherry was delivered bilaterally whereas lentiviruses encoding EGFP or Cre:EGFP were each delivered unilaterally to the VMHvl of $Esr1^{Flox/Flox}$ females.

(H) Fewer mCherry+ presynaptic termini apparent in AVPV of female on the side that received Cre:EGFP (right) compared to the side that received EGFP (left)

(I) Fewer mCherry+ presynaptic termini in AVPV upon deletion of Esr1 in ipsilateral VMH. Change in density represented as fold change compared to control (EGFP) side.

Mean ± SEM. n = 4 (Vehicle), 10 (Estrogen) (C), n = 3/genotype (F), n = 6 (I). Scale bar = 10 μm. *p<0.05, **p<0.01.

See also Figure S7.

KEY RESOURCE TABLE

REAGENT or RESOURCE	SOURCE	IDENTIFIER
Antibodies		
Rat anti-RFP	Chromotek	Cat #: 5f8; RRID: AB_2336064
Rabbit anti-Fos	Santa Cruz Biotechnology	Cat #: SC52; RRID: AB_2106755
Chicken anti-β-galactosidase	Abcam	Cat #: 9361; RRID: AB_307210
Sheep anti-GFP	BioRad	Cat #: 4745-1051; RRID: AB_619712
Rat anti-mCherry	Life Sciences	Cat #: M11217; RRID: AB_2536611
Rabbit anti-Esr1	Millipore	Cat #: 06-935; RRID: AB_310305
Guinea Pig anti-vGlut2	Synaptic Systems	Cat #: 135 404; RRID: AB_887884
Donkey anti-Rat, Cy3 conjugate	Jackson immunoResearch	Cat # 712-165-150; RRID: AB_2340666
Donkey anti-Rabbit, Alexa Fluor 488 conjugate	Jackson immunoResearch	Cat #: 711-545-152; RRID: AB_2313584
Donkey anti-Chicken, Cy3 conjugate	Jackson immunoResearch	Cat #: 703-165-155; RRID: AB_2340363
Donkey anti-Sheep, Alexa Fluor 488 conjugate	Jackson immunoResearch	Cat # 713-545-147; RRID: AB_2340745
Donkey anti-Guinea Pig, Alexa Fluor 647 conjugate	Jackson immunoResearch	Cat #: 706-605-148; RRID: AB_2340476
Bacterial and Virus Strains		
AAV1-EF1a-flex-hM3DDq-mCherry	UNC Vector Core; plasmid a gift from Bryan Roth	Addgene number: 50460
AAVDJ-EF1a-flex-hM3DDq-mCherry	UNC Vector Core; plasmid a gift from Bryan Roth	Addgene number: 50460
AAV1-EF1a-flex-hM4DDi-mCherry	UNC Vector Core; plasmid a gift from Bryan Roth	Addgene number: 50461
AAVDJ-EF1a-flex-hM4DDi-mCherry	UNC Vector Core; plasmid a gift from Bryan Roth	Addgene number: 50461
AAV1-EF1a-flex-mCherry	UNC Vector Core; plasmid a gift from Bryan Roth	Addgene number: 50462
AAV2-EF1a-DIO-hChR2(H134R):mCherry	UNC Vector Core; plasmid a gift from Karl Deisseroth	Addgene number: 20297
AAVDJ-EF1a-flex-taCasp3-TEVp	UNC Vector Core; (Yang et al., 2013)	Addgene number: 45580
AAV2-EF1a-DIO-eNpHR3.0:EYFP	UNC Vector Core; (Gradinaru et al., 2010)	Addgene number: 26966
AAV2-EF1a-DIO-EYFP	UNC Vector Core; plasmid a gift from Karl Deisseroth	Addgene number: 27056
AAV1-Syn-flex-GCaMP6s	Penn Vector Core; (Chen et al., 2013)	Addgene number: 100845
AAV1-EF1a-DIO-hChR2(H134R):EYFP	Penn Vector Core / Addgene; plasmid a gift from Karl Deisseroth	Addgene number: 20298
AAV8.2-EF1a-DO-Synaptophysin:mCherry	MGH Viral Core	Cat #: AAV-RN14
AAV8.2-EF1a-Synaptophysin:mCherry	MGH Viral Core	Cat #: AAV-RN8
AAV1-EF1a-DIO-Synaptophysin:mCherry	Virovek	N/A
AAVDJ-Syn-flex-mGFP-2A-Synaptophysin:mRuby	Virovek	Addgene number: 71760
Lenti-hSyn-Cre-EGFP	Stanford Viral Core	Cat #: LV-13
Lenti-hSyn-DCre-EGFP	Stanford Viral Core	Cat #: LV-14

REAGENT or RESOURCE	SOURCE	IDENTIFIER
Chemicals, Peptides, and Recombinant Proteins		
DAPI	Sigma-Aldrich	Cat # D9542; CAS 2871890-3
Clozapine-N-oxide (CNO)	Enzo Life Sciences	Cat # BML-NS105-0005
Estradiol	Sigma-Aldrich	Cat # E8875; CAS 50-28-2
Progesterone	Sigma-Aldrich	Cat # P0130; CAS 57-83-0
Critical Commercial Assays		
Estradiol ELISA Kit	Cayman	Cat #: 582251
Progesterone ELISA Kit	Cayman	Cat #: 582601
ACTH ELISA Kit	DRG	Cat #: EIA3647
Experimental Models: Organisms/Strains		
Mouse: C57BL/6J	The Jackson Laboratory	Cat # 000664; RRID: IMSR_JAX:000664
Mouse: B6129SF1/J	The Jackson Laboratory	Cat # 101043; RRID: IMSR_JAX:101043
Mouse: *PR*^{Cre}	Yang et al., 2013	Cat # 017915; RRID: IMSR_JAX: 017915
Mouse: *PR*^{PL}	Yang et al., 2013	Cat # 022517; RRID: IMSR_JAX: 022517
Mouse: *Esr1*^{flox}	Feng et al., 2007	N/A
Mouse: *Gad1*^{EGFP}	Tamamaki et al., 2003	N/A
Software and Algorithms		
ImageJ	NIH	https://imagej.nih.gov/ij/index.html; RRID: SCR_003070
Photoshop CS6	Adobe	https://www.adobe.com/products/photoshop.html; RRID: SCR_014199
MATLAB	MathWorks	https://www.mathworks.com/products.html; RRID: SCR 001622
GraphPad Prism 6	GraphPad Software	https://www.graphpad.com/scientificsoftware/prism/; RRID: SCR_002798